

**INVESTIGATION OF VARIOUS
SUBSTITUTION EFFECTS ON
BiPbSrCaCuO TYPE HIGH-
TEMPERATURE CERAMIC
SUPERCONDUCTORS**

119619

**T.C. YÜKSEKÖĞRETİM KURULU
DOKÜMANTASYON MERKEZİ**

by

Serpil ŞAKİROĞLU

March, 2002

İZMİR

119619

**INVESTIGATION OF VARIOUS
SUBSTITUTION EFFECTS ON
BiPbSrCaCuO TYPE HIGH-
TEMPERATURE CERAMIC
SUPERCONDUCTORS**

**A Thesis Submitted to the
Graduate School of Natural and Applied Sciences of
Dokuz Eylül University
In Partial Fulfillment of the Requirements for
The Degree of Master of Science in Physics**

by

Serpil ŞAKİROĞLU

March, 2002

İZMİR

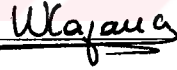
M.Sc. THESIS EXAMINATION RESULT FORM

We certify that we have read this thesis, entitled “**INVESTIGATION OF VARIOUS SUBSTITUTION EFFECTS ON BiPbSrCaCuO TYPE HIGH-TEMPERATURE CERAMIC SUPERCONDUCTORS**” completed by **Serpil ŞAKİROĞLU** under supervision of **Prof. Dr. Kemal KOCABAŞ** and that in our opinion it is fully adequate, in scope and in quality, as a thesis for the degree of Master of Science.



Prof. Dr. Kemal KOCABAŞ
Supervisor

Prof. Dr. Nadide KAZANCI



Committee Member

Prof. Dr. Binyamin ÖZBAY



Committee Member

Approved by the
Graduate School of Natural and Applied Sciences


Prof. Dr. Cahit Helvacı

Director

ACKNOWLEDGMENTS

I wish to express my sincere gratitude to my supervisor Prof. Dr. Kemal KOCABAŞ for his continual presence, invaluable guidance and boundless enthusiasm throughout the course of this work.

I am also grateful to the Director of Ankara Nuclear Research and Training Center Assoc. Prof. İsmail Ercan for his continual encouragement and technical support for R-T measurements all throughout the work.

Serpil ŞAKİROĞLU

ABSTRACT

In this work, elemental substitutional effects on the structural and superconducting properties of $\text{Bi}_{1.7}\text{Pb}_{0.3}\text{Sr}_2\text{Ca}_{2-x}\text{M}(\text{Zn,Ag})_x\text{Cu}_3\text{O}_y$ system were investigated. Our aim was an investigation the effects of substitution of elements with different ionic radii respect to replaced element.

Partial molar replacement of Ca by ZnO and Ag_2O was investigated in $x=0.00 - 0.20$ substitutional range. Samples prepared with conventional solid state reaction method were sintered at 850°C after pressed under 375 MPa pressure.

Critical temperatures of samples were determined by resistivity-temperature measurements made in liquid nitrogen conditions. XRD measurements were done by powder x-ray diffraction method. Data on the granular structure of samples were obtained from scanning electron microscope (SEM) photographs with X2000 magnification. Additional data about properties of the system was observed by density measurements made by Archimedes water displacement method and by calculations of volume fraction of high- T_c phase obtained from XRD results.

T_c values for ZnO substituted samples are in 95-110 K range while for Ag_2O substituted samples are in 106-115 K range. All samples in both substitutional group, show narrow transition width which gives information about purity of samples.

X-ray diffraction datum indicates that samples have multiphase structure and contain 2223 phase as main phase. Volume fraction results, calculated with

intensities of L(008) and H(0010) peaks, in both group increase with substitutional ratio, but have higher value for Ag₂O group.

The density values for all samples are almost same and are less than the theoretical density. Smaller density is sign of the less compact form and pores between grains. Comparison of SEM microphotographs indicates that in both group plate-like grain alignment is dominant. But for Ag₂O substitution samples higher grain size provides stronger contact, which improves superconducting properties.

Substituted elements have different ionic radii than Ca, ionic radii of ZnO is smaller while Ag₂O's is higher. This difference of ionic radii may be responsible for variation of the structure of system. Results show that Ag₂O plays better role in improvement of the superconducting properties than the ZnO.

ÖZET

Bu çalışmada $\text{Bi}_{1.7}\text{Pb}_{0.3}\text{Sr}_2\text{Ca}_{2-x}\text{M}(\text{Zn,Ag})_x\text{Cu}_3\text{O}_y$ sisteminin yapısal ve superiletkenlik özellikleri üzerine elemental katkılama etkileri incelenmiştir. Amacımız, yerdeğiştirilen elemente göre farklı iyonik yarıçaplara sahip elementlerin katkılama etkilerini incelemektir.

Ca'un ZnO ve Ag_2O ile kısmi yerdeğiştirmesi $x=0.00-0.20$ katkılama oranı aralığında araştırılmıştır. Katıhal reaksiyon yöntemiyle hazırlanan örnekler 375 MPa basınç altında preslendikten sonra 850°C 'de sinterlenmiştir.

Örneklerin kritik sıcaklıkları sıvı azot ortamında yapılan özdirenç-sıcaklık ölçümleriyle belirlenmiştir. XRD ölçümleri x-ışını toz diffraksiyon yöntemiyle yapılmıştır. Örneklerin tanecikli yapısı hakkındaki veriler X2000 büyütme taramalı electron mikroskobu (SEM) fotoğraflarından elde edilmiştir. Sistem özellikleri hakkındaki diğer veriler Archimedes su yerdeğiştirme yöntemi ile yapılan yoğunluk ölçümleri ile XRD sonuçlarından elde edilen yüksek- T_c fazı hacim kesri hesaplamalarından bulunmuştur.

Ag_2O katkılı örnekler için T_c değerleri 106-115 K aralığında iken ZnO katkılı örnekler için 95-110 K aralığındadır. Örneklerin saflığı hakkında bilgi veren geçiş aralığı her iki katkı grubundaki tüm örnekler için dar bir aralığa sahiptir.

X-ışını diffraksiyon sonuçları örneklerin çokfazlı bir yapıya sahip olduğunu ve ana faz olarak 2223 fazının var olduğunu göstermiştir. L(008) ve H(0010) piklerinin

şiddetleri kullanılarak hesaplanan hacim kesri sonuçları her iki grup için katkılama oranı ile artmıştır, ancak Ag_2O grubu için daha büyük değerlere sahiptir.

Tüm örnekler için yoğunluk değerleri hemen hemen aynıdır ve teorik değerden daha küçüktür. Daha küçük bir yoğunluk daha az sıkı formun ve tanecikler arası gözeneklerin varlığının işaretidir. SEM mikrofotograflarının karşılaştırılması her iki grupta düzlemsel tanecik diziliminin baskın olduğunu göstermektedir. Fakat Ag_2O katkılı örneklerin daha büyük tanecik ölçüleri, süperiletkenlik özellikleri iyileştiren daha güçlü kontağı sağlarlar.

Katkılanan elementler Ca'a göre farklı iyonik yarıçaplara sahiptir, ZnO 'in iyonik yarıçapı daha küçük iken Ag_2O 'nin yarıçapı daha büyüktür. Yarıçaplardaki bu farklılık sistemin yapısındaki değişimden sorumlu olabilir. Sonuçlar Ag_2O 'nin ZnO 'e göre süperiletkenlik özelliklerinin iyileşmesinde daha iyi bir rol oynadığını göstermektedir.

CONTENTS

	Page
Contents.....	IX
List of Figures.....	XII
List of Tables.....	XV

Chapter One

INTRODUCTION AND OVERVIEW

1.1. Introduction.....	1
1.2. The Phenomenon of Superconductivity.....	3
1.2.1. A Brief History.....	3
1.2.2. Types of Superconductors and Some Properties of Them.....	5
1.2.2.1. Type-I Superconductors.....	5
1.2.2.2. Type-II Superconductors.....	9
1.2.2.3. Specific Heat.....	14
1.2.2.4. Microscopic Theory of Superconductivity.....	15
1.2.2.5. Tunneling.....	19
1.2.3. High Temperature Superconductors.....	24
1.2.3.1. Crystal Structure.....	24
1.2.3.1.1. Crystal Structure of $\text{Bi}_2\text{Sr}_2\text{CuO}_{6+x}$	25
1.2.3.1.2. Crystal Structure of $\text{Bi}_2\text{Sr}_2\text{CaCu}_2\text{O}_{8+x}$	26
1.2.3.1.3. Crystal Structure of $\text{Bi}_2\text{Sr}_2\text{Ca}_2\text{Cu}_3\text{O}_{10+x}$	27
1.2.3.2. Characterization.....	27

1.2.3.2.1. Electrical Properties.....	29
1.2.3.2.2. Crystal Structures.....	29
1.2.3.2.3. Microstructures.....	31

Chapter Two

EXPERIMENTAL DETAILS

2.1. Preparation of Samples.....	32
2.2. Characterization of Samples.....	34
2.2.1. Resistivity Measurements.....	34
2.2.2. X-ray Diffraction Measurements.....	35
2.2.3. Scanning Electron Microscopy (SEM) Measurements.....	37
2.3. Effects of Substitution and Doping in BSCCO system.....	38
2.3.1 Formation of Bi-2223 Phase.....	38
2.3.2 Effect of Dopant and Substitution.....	39
2.3.2.1 Effect of Zn.....	40
2.3.2.2 Effect of Ag.....	40

Chapter Three

EXPERIMENTAL RESULTS

3.1. Experimental Procedure of Preparation of Samples.....	42
3.2. Effect of Zinc oxide Substitution.....	43
3.2.1. Resistivity Measurements.....	43
3.2.2. X-ray Diffraction Measurements.....	45
3.2.3. SEM Measurements.....	49
3.3. Effect of Silver (II) oxide Substitution.....	52
3.3.1. Resistivity Measurements.....	52
3.3.2. X-ray Diffraction Measurements.....	55

3.3.3. SEM Measurements.....	60
3.4. Comparison of Results.....	63

Chapter Four

CONCLUSIONS

4.1. Conclusions.....	66
Appendices.....	67
References	69

LIST OF FIGURES

		Page
Figure 1.1.	Resistivity behaviour of a superconductor.....	3
Figure 1.2.	Historical evolution of superconductivity.....	5
Figure 1.3.	A type-I superconductor in the form of a long cylinder in the presence of an external magnetic field.....	6
Figure 1.4.	Variation of flux density at boundary of a superconductor....	7
Figure 1.5.	Phase diagram of a superconductor, showing variation with temperature of the critical magnetic field.....	9
Figure 1.6.	Penetration depth and coherence range at boundary between normal and superconducting regions.....	9
Figure 1.7.	A schematic diagram of a type-II superconductor in the vortex state.....	10
Figure 1.8.	Sketch of the magnetic field around an individual vortex.....	11
Figure 1.9.	Critical magnetic fields as a function of temperature for type-II superconductors.....	12
Figure 1.10.	T-B-J phase diagram for type-II superconductor. The resistive state is bounded by a surface, which depends on specimen geometry.....	13
Figure 1.11.	Specific heat in normal and superconducting states.....	14
Figure 1.12.	Basis for the attractive interaction between two electrons via lattice deformation.....	16
Figure 1.13.	Schematic representation of electron-electron interaction transmitted by a phonon.....	17

Figure 1.14.	Occurrence of Cooper pair formation around E_F , and Boson condensation of Cooper pairs onto Δ , the Boson level after phononic interaction over the electronic range $2\hbar\omega_d$ around E_F	18
Figure 1.15.	I-V behaviour of Josephson junction where 2Δ is energy gap of superconductor.....	20
Figure 1.16.	Model for superconductor-metal tunneling with applied voltages of (a) $V=0$, (b) $V=\Delta/e$ and (c) $V=-\Delta/e$. Occupied states are cross-hatched below Fermi energy. SIS tunneling current grows when (d) $V \geq 2\Delta/e$. \circ denotes Cooper pair and \bullet normal electron.....	21
Figure 1.17.	(a) Supercurrent dividing through two weak links suffers phase change $\Delta\theta$ due to applied potential. (b) Magnetic flux induces additional circulating supercurrent, which suffers phase changes $+\delta$ and $-\delta$ at the junctions. (c) Measurement of the resulting supercurrent in a low T_c SQUID interferometer shows interference in current transport.....	22
Figure 1.18.	Crystal structure of $\text{Bi}_2\text{Sr}_2\text{CuO}_6$ system.....	26
Figure 1.19.	Crystal structure of (a) $\text{Bi}_2\text{Sr}_2\text{CaCu}_2\text{O}_8$ and (b) $\text{Bi}_2\text{Sr}_2\text{Ca}_2\text{Cu}_3\text{O}_{10}$ systems.....	28
Figure 1.20.	Powder X-ray diffraction patterns (CuK_α) of single phase BSCCO system. [$n=1$ (2201); $n=2$ (2212); $n=3$ (2223)].....	30
Figure 2.1.	Solid-state reaction method procedure for producing BPSCCO.....	33
Figure 2.2.	Schematic four-probe resistance apparatus with temperature sensor used for measuring dc resistivity.....	34
Figure 2.3.	Cryogenic system for the measurement of resistivity.....	35
Figure 2.4.	Schematic illustration of the formation of a cone of diffracted radiation from a given lattice plane in the powder diffraction method.....	36
Figure 3.1.	Flowchart of the solid-state reaction method.....	43

Figure 3.2.	Resistivity versus temperature of ZnO substituted samples. A(x=0.00), B(x=0.05), C(x=0.10), D(x=0.15), E(x=0.20).....	44
Figure 3.3.	XRD patterns of ZnO substituted samples of $\text{Bi}_{1.7}\text{Pb}_{0.3}\text{Sr}_2\text{Ca}_{2-x}\text{Zn}_x\text{Cu}_3\text{O}_y$ system. [A(x=0.00), B(x=0.05), C(x=0.10), D(x=0.15), E(x=0.20)] ○- Low- T_c phase; ●- High- T_c phase; □- ZnO; * - CuO.....	46
Figure 3.4.	Volume fraction of ZnO substituted samples.....	48
Figure 3.5.	a) Scanning electron microscope photographs of the top surfaces of ZnO substituted samples. Magnification X 2000. [A(x=0.00), B(x=0.05), C(x=0.10)].....	50
Figure 3.5.	b) Scanning electron microscope photographs of the top surfaces of ZnO substituted samples. Magnification X 2000. [D(x=0.15), E(x=0.20)].....	51
Figure 3.6.	Resistivity curves of Ag_2O substituted samples.....	53
Figure 3.7.	a) XRD patterns of Ag_2O substituted samples of $\text{Bi}_{1.7}\text{Pb}_{0.3}\text{Sr}_2\text{Ca}_{2-x}\text{Ag}_x\text{Cu}_3\text{O}_y$ system. [A (x=0.00), B (x=0.05)] ○- Low- T_c phase; ●-High- T_c phase; * - CuO; Δ-unknown phase.....	56
Figure 3.7.	b) XRD patterns of Ag_2O substituted samples of $\text{Bi}_{1.7}\text{Pb}_{0.3}\text{Sr}_2\text{Ca}_{2-x}\text{Ag}_x\text{Cu}_3\text{O}_y$ system. [C (x=0.10), D (x=0.15)] ○- Low- T_c phase; ●-High- T_c phase; * - CuO; Δ-unknown phase.....	57
Figure 3.7.	c) XRD patterns of Ag_2O substituted samples of $\text{Bi}_{1.7}\text{Pb}_{0.3}\text{Sr}_2\text{Ca}_{2-x}\text{Ag}_x\text{Cu}_3\text{O}_y$ system. [E (x=0.20)] ○- Low- T_c phase; ●-High- T_c phase; * - CuO; Δ - unknown phase.....	58
Figure 3.8.	Volume fraction of Ag_2O substituted samples.....	59
Figure 3.9.	a) Scanning electron microscope photographs of the top surfaces of Ag_2O substituted samples. Magnification X 2000. [A(x=0.00), B(x=0.05), C(x=0.10)].....	61
Figure 3.9.	b) Scanning electron microscope photographs of the top surfaces of Ag_2O substituted samples. Magnification X 2000. [D(x=0.15), E(x=0.20)].....	62

LIST OF TABLES

	Page
Table 3.1. Comparison of characteristics obtained for ZnO and Ag ₂ O substituted samples.....	65



CHAPTER ONE

INTRODUCTION AND OVERVIEW

1. 1. Introduction

In 1911, Heike Kamerling Onnes discovered superconductivity (the ability of a metal to carry electricity with no resistance) in mercury, cooled by expensive and rare liquid helium to below the critical temperature (T_c) of 4.2 K(Kelvin). During the next 75 years, applications were developed, such as powerful magnets built of superconducting materials for medical magnetic resonance imaging(MRI), high energy accelerators like the proposed Superconducting Supercollider (SSC), and very sensitive magnetic field detectors called Superconducting Quantum Interference Devices (SQUIDs). Because of the expense and inconvenience of liquid helium refrigeration, however, other applications of the phenomenon were not considered economically feasible.

In April 1986, two researchers at IBM in Switzerland, K.Alex Muller and George Bednorz, detected superconductivity in $(La-Ba)_2CuO_4$ with a T_c up to 35 K, in contrast to the previous record of 23 K for which they were subsequently awarded the Nobel Prize. By the end of 1986, superconductivity research achieved revolutionary advances with the the effort of W.Chu and colleagues at the University of Houston. Signs of superconductivity above 77 K were repeatedly observed in poorly-characterized samples during the period, strongly affirming the belief in the existence of superconductivity in the liquid-nitrogen temperature range. The scientific world knew that the textbooks had to be rewritten after January 1987, when the Houston group in collaboration with M.K.Wu, Chu's former student, achieved stable and reproducible superconductivity above 90 K in $YBa_2Cu_3O_{7-d}$ (Y123), with

(Y123), with T_c close to 100 K. The recent discovery of superconductivity in magnesium diboride (MgB_2 -2001) with T_c as 39 K caused excitement in the Solid State Physics community. (MgB_2) is a new simple intermetallic superconductor with a high superconducting transition temperature for a nonoxide and non C_{60} based compound. The reported value of T_c seems to be either above or at the limit suggested theoretically for BCS, phonon mediated superconductivity (Kazakov et al.,2001).

In addition to the savings in cost resulting from the displacement of liquid helium by liquid nitrogen for cooling, it is now apparent that superconductivity applications with more inexpensive refrigerants are possible. The race for new superconductors with higher T_c continues. Bismuth and thallium superconducting systems were discovered in 1988 which superconduct at 110 K and 125 K, respectively. The mercury-based compound was discovered in 1993, with temperatures up to 164 K under pressure, another world record set at Houston.

The observation of superconductivity above 77 K in such unusual classes of materials defied the predictions of earlier theories; but these materials are also intriguing because they behave unusually above their T_c 's as well; e.g. the *Meissner effect*. The causes for and consequences of these observations pose great challenges to physicists, chemists and material scientists. Even though "the liquid nitrogen barrier" has been broken, many of the great promises of superconductivity technology have yet to be realised. The difficulties with the materials can be attributed to many of the material and engineering problems of HTSC's, e.g. making long HTSC wire than can carry large current without energy loss and can retain excellent superconducting properties over long periods of time without chemical and physical degradation.

However, commercial applications of HTSC technology field such as electric power, transportation, electronics and medicine are now appearing. Current applications of HTSC include thin films, magnetic resonance imaging (MRI), wireless communication filters and ultra-fast computer chips. By the year 2010, it is estimated that the global superconductivity market will be in excess of \$50 million.

1. 2. The Phenomenon of Superconductivity

1. 2. 1. A Brief History

A perfect superconductor is a material that exhibits two characteristic properties, namely zero electrical resistance and perfect diamagnetism, when it is cooled below a particular temperature T_c , called the *critical temperature*. At higher temperatures it is a normal metal, and ordinarily is not a very good conductor. For example, lead, tantalum, and tin become superconductors, while copper, silver, and gold, which are much better conductors, do not superconduct. In the normal state some superconducting materials are weakly diamagnetic and some are paramagnetic. Below T_c they exhibit perfect electrical conductivity and also perfect or quite pronounced diamagnetism.

In 1908, H.Kamerling Onnes initiated the field of low-temperature physics by liquifying helium in his laboratory at Leiden. Three years later he found that below 4.15 K of the dc resistance of mercury dropped to zero. With that finding the field of superconductivity was born. Five years later, in 1913, the element lead was found to be superconducting at 7.2 K (Uluğ, 1994).

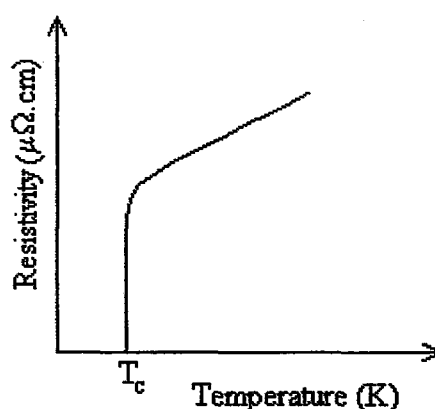


Figure 1.1. Resistivity behaviour of a superconductor.

A considerable amount of time went by before physicists became aware of the second distinguishing characteristic of a superconductor – namely, its perfect diamagnetism. In 1933, Meissner and Ochsenfeld discovered that when a sphere is cooled below its transition temperature in a magnetic field, it excludes the magnetic

flux from the interior of a superconductor. This as encountered on cooling is now called *Meissner effect*. The report of Meissner effect led the London brothers, Fritz and Heinz, to propose equations that explain this effect and predict how far a static external magnetic field can penetrate into a superconductor. The next theoretical advance came in 1950, with the theory of Ginzburg and Landau, which described superconductivity in terms of an order parameter and provided a derivation for the London equations.

In the same year it was predicted theoretically by H.Fröhlich that the transition temperature would decrease as the average isotopic mass increased. This effect, called the *isotope effect*, provided support for the electron-phonon interaction mechanism of superconductivity, was observed experimentally the same year.

In 1957 Bardeen, Cooper and Schrieffer (BCS) proposed a microscopic theory of superconductivity that predicts quantitatively many of the properties of elemental superconductors. In addition, the Landau-Ginzburg theory, with the added bonus that the charge and mass of the “particle” involved in the superconducting state emerge naturally as $2e$ and $2m_e$, respectively. In this theory it is assumed that bound electron pairs that carry the super current are formed and that an energy gap between the normal and superconductive states is created.

In 1986, Bednorz and Müller at IBM Zurich Research Laboratory discovered a new outstanding superconductor with a critical temperature T_c of 30 K in the La-Ba-Cu-O (LBCO) system. Late in 1986, Tanaka’s group at the University of Tokyo, demonstrated that the substitution of Sr for Ba worked to increase T_c as high as 42.5 K. After a little silence on high- T_c information, on February 1987, Wu et al. at the University of Alabama and the University of Houston discovered superconductivity at 90 K, above liquid-nitrogen temperature, in the Y-Ba-Cu-O (YBCO) system. Early in 1988 Maeda and Michel et al. found a sample showing stepwise two transitions in the electrical resistance-temperature curve measured by the standard four-probe method. The high transition exhibiting an onset temperature of 114 K and a projected zero resistance value of approximately 105 K and the lower one at about 80 K. The

sample had a nominal composition of BiSrCaCuO. More recently, Berkley et al. (1993) reported $T_c=131.8$ K for $Tl_2Ba_2Ca_2Cu_3O_{10-x}$ at a pressure of 7 GPa. Several researchers have reported T_c above 130 K for the Hg series of compounds $HgBa_2Ca_nCu_{n+1}O_{2n+4}$ with $n=1,2..$ sometimes with Pb doping for Hg.

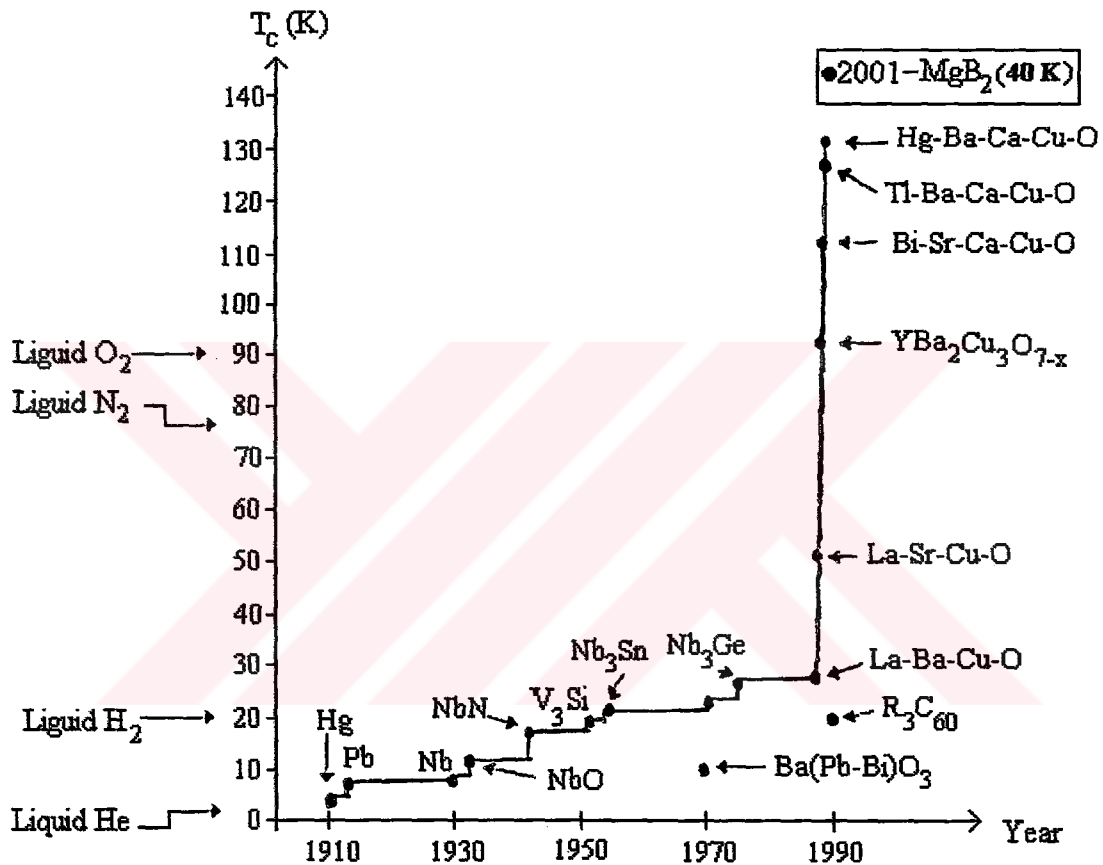


Figure 1.2. Historical evolution of superconductivity.

1. 2. 2. Types of Superconductors and Some Properties of Them

1. 2. 2. 1. Type-I Superconductors

According to their magnetic properties, superconductors are divided into type-I and type-II superconductors. Type-I superconductors include all superconducting elements except niobium. Niobium, superconducting alloys and chemical compounds

make up the second group, type-II superconductors. The so-called high- T_c superconductors also belong to this group.

The essential difference between the two groups lies in their different response to an external magnetic field. The Meissner-Ochsenfeld effect is observed in type-I superconductors only. Type-I superconductors, with a positive interface energy, show a reversible first-order phase transition with a latent heat when the applied magnetic field reaches B_c ; an at this particular field relatively thick normal and superconducting domains running parallel to the field can coexist, in what is known as the *intermediate state*. A metal in the superconducting state never allows a magnetic flux density to exist in its interior. When a superconductor is cooled in a weak magnetic field, at the transition temperature persistent screening currents arise on the surface and circulate so as to cancel the flux density inside, in just the same way as when a magnetic field is applied after the metal has been cooled. This effect, whereby a superconductor never has a flux density inside even when in an applied magnetic field, is called *the Meissner effect* as shown in Figure 1.3(Waldram, 1996).

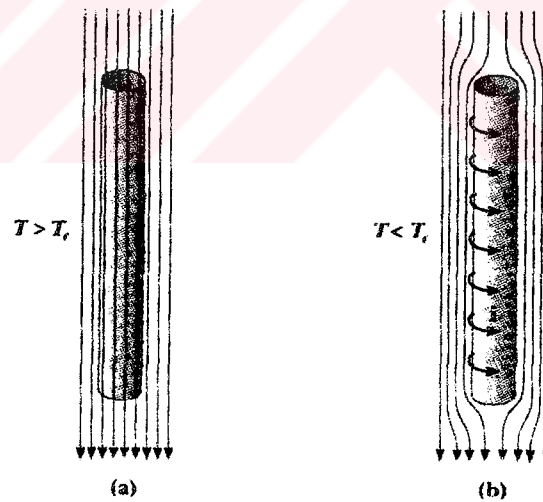


Figure 1.3. A type-I superconductor in the form of a long cylinder in the presence of an external magnetic field.

The strength H_0 of the applied external magnetic field is given by

$$H_0 = B_0 / \mu_0 \quad (1.1)$$

and the flux density in a magnetic material is related to the strength of the applied field by

$$B = \mu_0(H_0 + M) \quad (1.2)$$

where M is the magnetization of the material. The magnetization of a superconductor, in which $B=0$, must therefore be

$$M = -H_0 \quad (1.3)$$

and the magnetic susceptibility, i.e. the ratio of the magnetization to the field strength, must be

$$\chi = -1 \quad (1.4)$$

When a superconducting sample is in an applied magnetic field, the screening currents, which circulate to cancel the flux inside, must flow within very thin surface layer. Consequently, the flux density does not fall abruptly to zero at the boundary of the metal but dies away within the region where the screening currents are flowing. For this reason the depth within the currents flow is called the *penetration depth* (λ), because it is the depth to which the flux of the applied external magnetic field appears to penetrate.

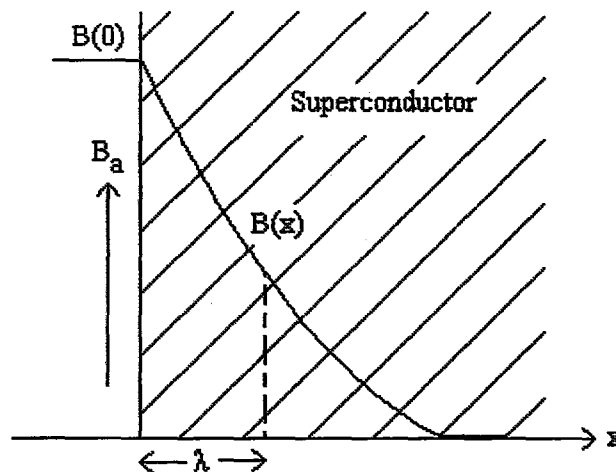


Figure 1.4. Variation of flux density at boundary of a superconductor.

The London theory of superconductivity predicts that in a specimen which is much thicker than the penetration depth the magnetic flux density decays exponentially as it penetrates into the metal,

$$B(x) = B(0) e^{-x/\lambda} \quad (1.5)$$

Where $B(0)$ is the flux density at the surface of the metal and λ is London penetration depth which is typically about 50 nm for type-I superconductors (Schmidt, 1997).

The penetration depth does not have a fixed value but varies with temperature. At low temperatures it is nearly independent of temperature and has a value λ_0 characteristic of the particular value. Above about 0.8 of the transition temperature, however, the penetration depth increases rapidly and approaches infinity as the temperature approaches the transition temperature T_c . The variation of penetration depth with temperature is found to fit very closely the relation

$$\lambda = \lambda_0 / [1 - (T/T_c)^4]^{1/2} \quad (1.6)$$

If a metal is to remain superconducting, the net momentum of the superelectrons must not exceed a certain value. For this reason there is a limit to the density of resistanceless current J_c that can be carried by any region in the metal. As a result of this critical current density, a superconducting metal will be driven normal if a sufficiently strong magnetic field, called thermodynamic critical field B_c is applied to it. In the normal region above the transition temperature there is no critical field ($B_c = 0$) and there is a total magnetic field penetration ($\lambda = \infty$). As a superconductor is cooled down through the transition temperature T_c , the critical field gradually increases to its maximum value $B_c(0)$ at absolute zero ($T=0$), while the penetration depth decreases from infinity to its minimum value $\lambda(0)$ at absolute zero. The temperature dependence of critical field can be given by expression

$$B_c = B_c(0)[1 - (T/T_c)^2] \quad (1.7)$$

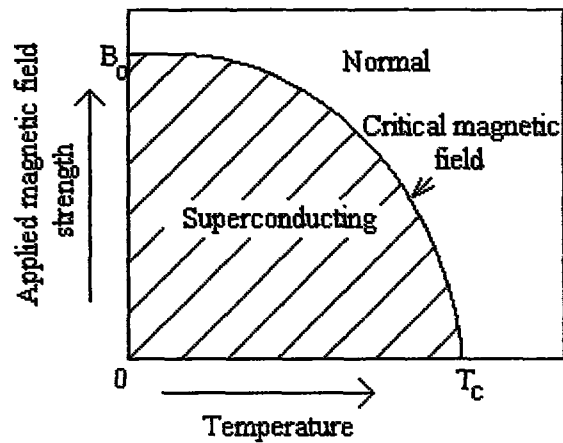


Figure 1.5. Phase diagram of a superconductor, showing variation with temperature of the critical magnetic field.

1. 2. 2. 2. Type-II Superconductors

Type-I superconductors that exhibit zero resistance are also perfect diamagnets for applied magnetic fields below the critical field B_c , and become normal in higher magnetic fields. When a superconductor is cooled below the transition temperature some extra form of order sets in amongst the conduction electrons, so a superconductor can be regarded as consisting of two interpenetrating electronic fluids, the normal electrons and the superelectrons. The superelectrons in some way possess greater order than the normal electrons, and we can think of degree of order of superconducting phase as being identified with the density of superconducting electrons (n_s). n_s cannot change rapidly with position, but can only change appreciably within a distance which for pure superconductors is of order of 10^{-4} cm. This distance is called *coherence length* (ξ).

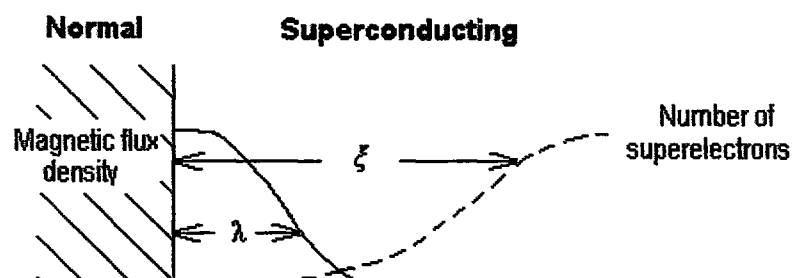


Figure 1.6. Penetration depth and coherence range at boundary between normal and superconducting regions.

One consequence of the existence of the coherence length is that, the boundary between a normal and superconducting region cannot be sharp, because the density of superelectrons can rise from zero in the normal region to its density n_s in the superconducting region only gradually over a distance equal to about the coherence length as shown in Figure 1.6 (Bourdillon&Bourdillon, 1994). An important property of the coherence length is that it depends on the purity of the metal. Their coherence length exceeds their penetration depth so it's not energetically favorable for boundaries to form between their normal and superconducting phases.

When the penetration depth λ is larger than coherence length ξ , it becomes energetically favorable for domain walls to form between the superconducting and normal regions. When such a superconductor, called type-II, is in a magnetic field, the free energy can be lowered by causing domains of normal material containing trapped flux to form with low energy boundaries created between the normal core and the surrounding superconducting material. When the applied magnetic field exceeds a value referred to as the lower critical field B_{c1} , magnetic flux is able to penetrate in quantized units, called flux quantum Φ_0 , by forming cylindrically symmetric domains called *vortices* (Waldram, 1996).

$$\Phi_0 = \frac{h}{2e} = 2,06 \cdot 10^{-15} \text{ weber} \quad (1.8)$$

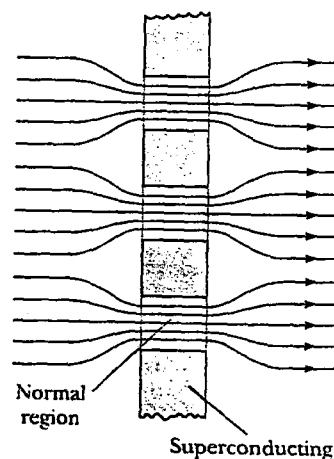


Figure 1.7. A schematic diagram of a type-II superconductor in the vortex state.

For applied fields slightly above B_{c1} , the magnetic field inside a type-II superconductor is strong in the normal cores of the vortices, decreases with distance from the cores, and becomes very small far away. For much higher applied fields the vortices overlap and the field inside the superconductor becomes strong everywhere. Eventually, when the applied field reaches a value called the upper critical field B_{c2} , the material becomes normal (Poole, Farach, & Creswick, 1995).

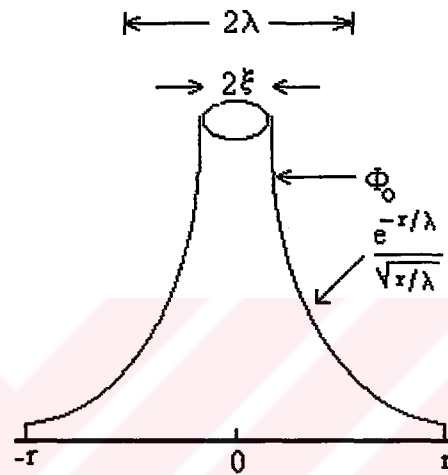


Figure 1.8. Sketch of the magnetic field around an individual vortex

Alloys and compounds exhibit type-II superconductivity, with mixed-type magnetic behaviour and partial flux penetration above B_{c1} . The superconductors used in practical applications, which have relatively high transition temperatures, carry large currents and often operate in large magnetic fields, are all of type-II.

There are two characteristic lengths whose relative ratio determines the type of the superconductivity in the magnetic field, the coherence length ξ and the penetration depth λ . Their ratio is the *Ginzburg-Landau parameter* κ ,

$$\kappa = \lambda / \xi \quad (1.9)$$

The density of super electrons n_s , which characterizes the superconducting state, increases from zero at the interface with a normal material to a constant value far inside, and the length scale for this to occur is the coherence length ξ . An external magnetic field B decays exponentially to zero inside a superconductor, with length

scale λ . The ratio κ has a critical value ($1/\sqrt{2}$) above which the superconductor is of type-II.

$$\kappa < 0.71 \text{ surface energy positive (Type I)} \quad (1.10)$$

$$\kappa > 0.71 \text{ surface energy negative (Type II)}$$

The *thermodynamic critical field* B_c , can be expressed as the difference $G_n - G_s$ in the Gibbs free energy between the normal and the superconducting states to the magnetic energy $B_c^2 / 2\mu_0$ of this critical field (Rose-Innes & Rhoderick, 1980),

$$G_n - G_s = B_c^2 / 2\mu_0 \quad (1.11)$$

In addition of this thermodynamic critical field, type-II superconductor has lower and upper critical fields, B_{c1} and B_{c2} , which are temperature dependent and can be expressed in terms of B_c

$$B_{c1} = \frac{B_c \ln \kappa}{\sqrt{2\kappa}} \quad (1.12)$$

$$B_{c2} = \sqrt{2\kappa} B_c \quad (1.13)$$

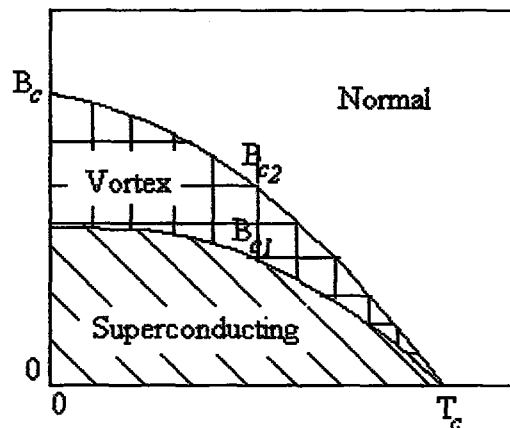


Figure 1.9. Critical magnetic fields as a function of temperature for type-II superconductors.

Defects, such as dislocations, precipitates of second phases, grain boundaries or voids, generally interact with the vortices, which have a core radius equal to the coherence length and a surrounding outer region with radius equal to the penetration depth. At field strengths $B_{c1} < B_c < B_{c2}$, in defect-free materials, the fluxoids move relatively easily through the superconductor to take up their equilibrium configuration, so the magnetization is reversible. Defects pin the fluxoids and prevent or restrict their movement. As the fields outside the superconductor and within it increase, fluxoids enter the material. Flux pinning causes flux entry delay, and the flux escape is inhibited when the field is reduced. The superconducting state can be represented, in type-II superconductors, on a phase diagram in T - B - J space as shown in Figure 1.10 (Bourdillon & Bourdillon, 1994).

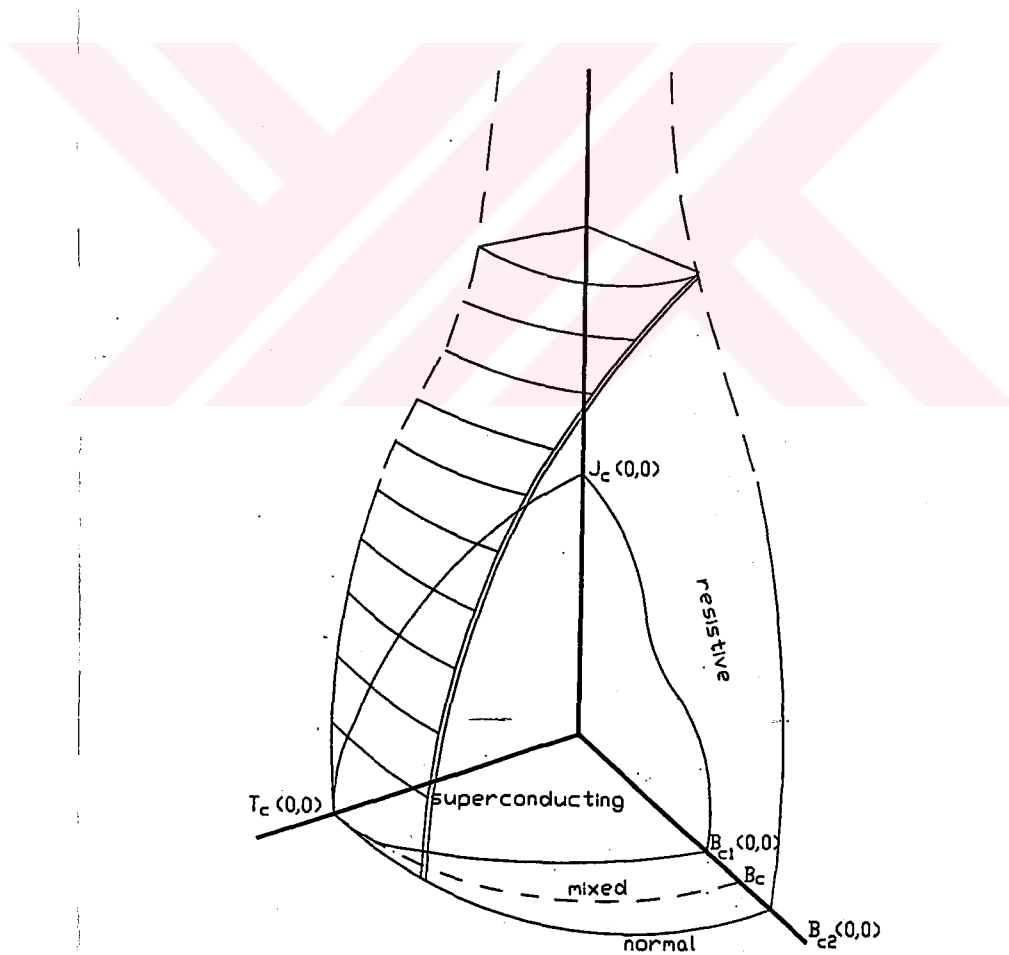


Figure 1.10. T - B - J phase diagram for type-II superconductor. The resistive state is bounded by a surface, which depends on specimen geometry.

1. 2. 2. 3. Specific Heat

Useful experiments to make on superconductors are heat capacity measurements. In treating the superconducting state it is convenient to make use of the free energy because (1) the superconductivity state is always the state of lowest free energy at particular temperature, and (2) the free energies of the normal and superconducting states are equal at the transition temperature. The free energy of the superconducting state can be derived from measurement of B_c . When $B=0$ there is no latent heat on cooling through the superconducting transition. This is a second order transition and so the specific heat is discontinuous at T_c as shown in Figure 1.11 (Kresin, 1990).

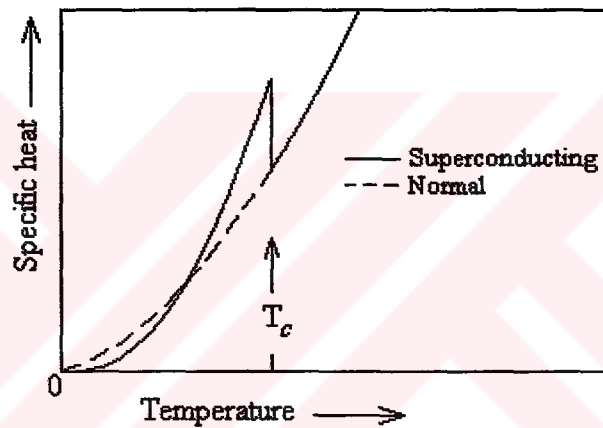


Figure 1.11. Specific heat in normal and superconducting states.

The lambda-shaped peak, shown inset, is subtracted from the measured specific heat after curve fitting at temperatures above and below T_c . The parts subtracted are the components of the specific heat due to the lattice, C_l , and to the normal electrons, C_n . The measured specific heat can be written as the sum (Bourdillon & Bourdillon, 1994).

$$C = C_s + C_l + C_n = C_s + A \left(\frac{T}{\Theta_D} \right)^3 + \gamma T n_n(T) \quad (1.14)$$

where C_s is the specific heat due to the superelectrons, A and γ are constants, Θ_D is the Debye temperature of the normal metal with density of normal electrons, n_n , changing with T . In the superconducting state the heat capacity varied roughly as T^3 ,

rising above the linear heat capacity of normal state as T_c was approached, and falling back to the normal value with a vertical discontinuity at T_c , with no latent heat at transition.

$$\frac{C_s - \gamma T_c}{\gamma T_c} = 1.43 \quad (1.15)$$

The heat capacity anomaly at T_c was of the sort usually associated with a higher-order phase transition involving an *ordering process*, like the appearance of ferromagnetism below the Curie temperature. This result suggested that superconductivity is due to the appearance below T_c of a group of electrons which have *condensed* into a new type of highly ordered quantum state, whose current, for some unknown reason, could not be removed gradually by the usual scattering mechanism. The absence of thermoelectric effects could be explained if the condensed electrons were so highly ordered as to carry no entropy.

1. 2. 2. 4. Microscopic Theory of Superconductivity

BCS Theory

In 1957 Bardeen, Cooper and Schrieffer proposed a microscopic theory of superconductivity that predicts quantitatively many of the properties of elemental superconductors. The BCS theory is based on the fact that the interaction between electrons resulting from virtual exchange of phonons is attractive when the energy difference between the electron states involved is less than the phonon energy, $\hbar\omega$. It is favorable to form a superconducting phase when this attractive interaction dominates the repulsive screened Coulomb interaction. The normal phase is described by the Bloch individual-particle model. The ground state of a superconductor, formed of a linear combination of normal state configurations in which electrons are virtually excited in pairs of opposite sign and momentum, is lower in energy than the normal state by an amount proportional to an average $(\hbar\omega)^2$, consistent with the isotope effect. A mutually orthogonal set of excited states in one-

to-one correspondence with those of the normal phase is obtained by specifying occupation of certain Bloch states and by using the rest to form a linear combination of virtual pair configurations.

A free electron may be represented by waves, and in an absolutely perfect crystal structure free from thermal vibrations (i.e. cooled to absolute zero), can propagate freely without attenuation, rather in the way in which an electric wave can pass along a lossless periodic filter without attenuation. However, if the perfect periodicity of the lattice is destroyed by thermal vibrations, the lattice behaves like a periodic filter in which the values of the some components fluctuate in a random manner. This causes a partial reflection of the wave, and in the same way an electron which encounters any departure from perfect periodicity of the crystal lattice would have a certain probability of being reflected, or scattered. Since the electrons are interacting with the atoms, this is called the electron-phonon (electron-lattice) interaction. In very poor metals (weakly delocalized) it is this interaction that determines the resistivity. In 1950 Fröhlich pointed out that the electron-phonon interaction provides a mechanism for a weak attraction between two electrons.

Represented in Figure 1.12. is how an electron (electron 1) will attract the positive ions around it, which move inward from their equilibrium positions showed in dashed circles (it is said that the electron polarizes the crystal).

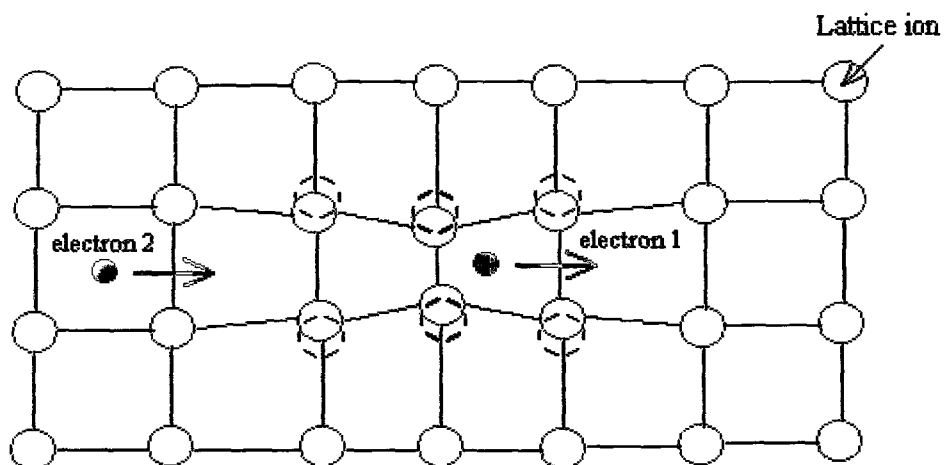


Figure 1.12. Basis for the attractive interaction between two electrons via lattice deformation.

This distorted region of the lattice has a net positive charge, and hence another electron (electron 2) in this general vicinity will be drawn toward this region because of the higher density of the positive charge. Hence, electrons are attracted to each other via the movement of the ions.

Figure 1.13.(Demirel, 1995) shows how this interaction is represented. An electron of wave vector \mathbf{k}_1 emits a phonon of wave vector \mathbf{q} and is scattered into a state with wave vector \mathbf{k}'_1 such that

$$\mathbf{k}_1 = \mathbf{k}'_1 + \mathbf{q} \quad (1.16)$$

In comparable manner this phonon is absorbed by a second electron, which changes its wave vector from \mathbf{k}_2 to \mathbf{k}'_2 .

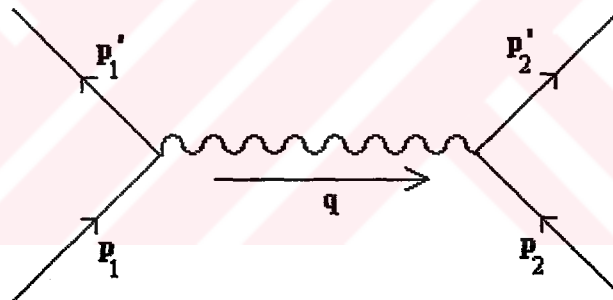


Figure 1.13. Schematic representation of electron-electron interaction transmitted by a phonon.

Both processes conserve crystal momentum, hence

$$\mathbf{k}_2 + \mathbf{q} = \mathbf{k}'_2 \quad (1.17)$$

and therefore

$$\mathbf{k}_1 + \mathbf{k}_2 = \mathbf{k}'_1 + \mathbf{k}'_2 \quad (1.18)$$

Thus an incoming electron of energy ε_k scattering on the lattice emits a phonon of energy $\hbar\omega$ that is then observed by another electron of energy ε'_k . This effective electron-electron interaction is given by

$$V_{kk'q} = |W_q| \frac{\hbar\omega_q}{(\varepsilon'_k - \varepsilon_k)^2 - (\hbar\omega)^2} \quad (1.19)$$

where W_q is electron-phonon matrix element (Demirel, 1995). Energy conservation during that process imposes the equality $\hbar\omega_q = \varepsilon_k - \varepsilon'_k$. However the interaction, as it occurred during a short time Δt , imposes an uncertainty on the particle's energy ΔE , such that the Uncertainty Principle given by $\Delta t \Delta E \approx \hbar$ is not violated. An attractive interaction results when $\hbar\omega_q > |\varepsilon_k - \varepsilon'_k|$.

If two extra electrons are added to an electron gas in a solid at $T = 0$ according to the Pauli Exclusion Principle they are positioned above the Fermi energy (Figure 1.14, Demirel, 1995).

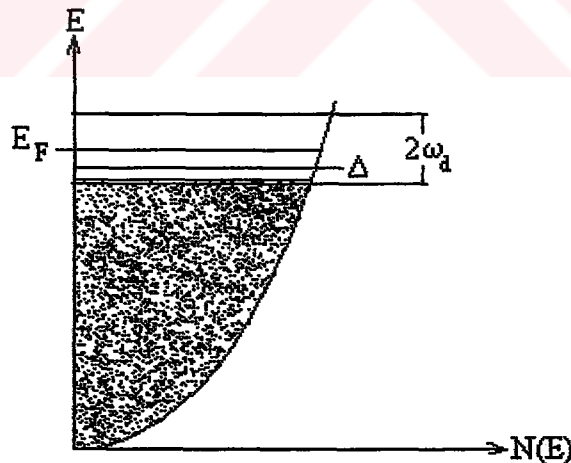


Figure 1.14. Occurrence of Cooper pair formation around E_F , and Boson condensation of Cooper pairs onto Δ , the Boson level after phononic interaction over the electronic range $2\hbar\omega_d$ around E_F .

Cooper showed that Eq.1.19 is approximated by a negative non-zero constant ($-V$) in the energy interval $2\hbar\omega_D$ around the Fermi energy, so that then a binding energy Δ is introduced between two electrons. $\hbar\omega_D$ the average phonon energy, which characterises the cut-off of the phonon spectrum, and $N(\epsilon_F)$ density of free particle states. Moreover it was found that the binding energy Δ is greatest when $\mathbf{k} + \mathbf{k}' = 0$ and the total spin is zero (singlet state).

As a result the total energy of the Cooper pair is smaller than for the equivalent electron set separately. This added stability drives the system to the lower ground state energy with the formation of a coherently condensed state of pairs in a superconducting phase at low temperatures.

1. 2. 2. 5. Tunneling

When, two metals are separated by a thin insulating layer it forms a potential barrier between the metals. Quantum mechanics predict that, if the layer is sufficiently thin, electrons can tunnel between the metals. If a voltage is applied across the metals the tunneling current is proportional to the applied voltage, following Ohm's law.

Tunneling in superconductors is technically valuable and also provides fundamental information about superconducting gap energies and other features. There are several types of tunneling, characterized by the nature of the barrier and of adjacent solids.

The tunneling of electrons between a metal and superconductor separated by a narrow insulating gap (air gap) . When a small voltage is applied, the current passed is close to zero, but it increases discontinuously at a certain applied voltage, and with further increase the I-V curve is ohmic (Kresin & Wolf, 1990).

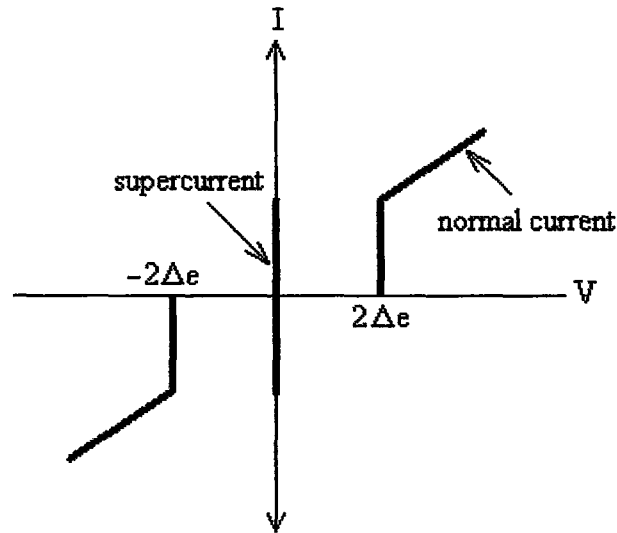


Figure 1.15. I-V behaviour of Josephson junction where 2Δ is energy gap of superconductor.

The discontinuity shows that the superconductor contains a band gap where the density of states equals to zero. When the potential applied across the air gap is equal to the energy of the superconducting band gap, Δ , transport begins. In low temperature superconductors the gap energies are much smaller and are related to respective T_c .

With forward bias $V \geq \Delta/e$ applied to the superconductor, electrons flow from the metal to the conduction band of the superconductor, as illustrated in Figure 1.16. In reverse bias, superconducting electrons conduct by going normal during tunneling. This occurs when $V \leq \Delta/e$, the energy gained in tunneling being used to excite a second superelectron into a normal electron state, which is an example of electron pair behaviour found to be general in superconductivity.

In a second type of tunneling, namely in superconductor-insulator-superconductor (SIS) junctions, conduction begins when $V = \Delta/e$. Figure shows schematically the break-up of a superelectron pair into two normal electrons. This I-V behaviour results from single particle tunneling.

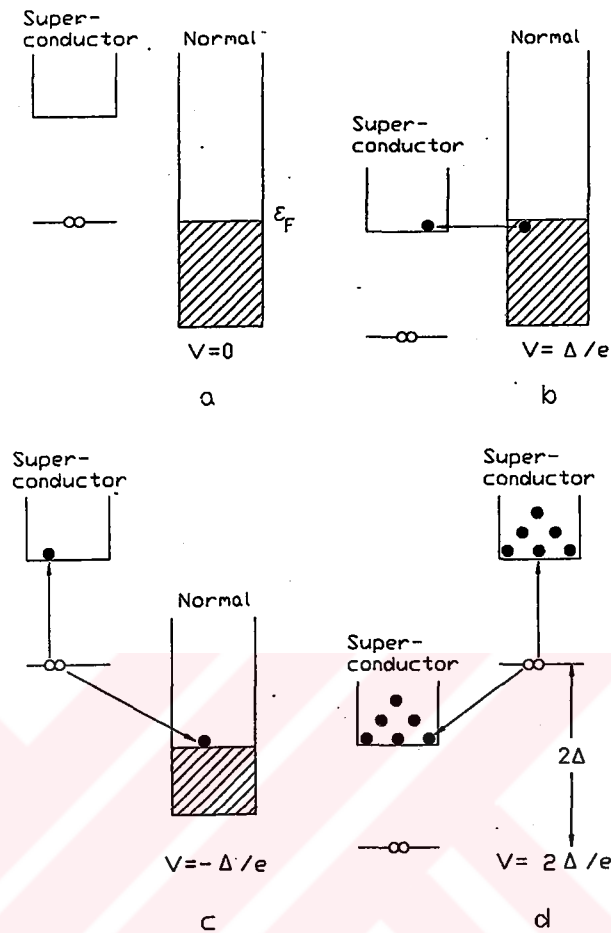


Figure 1.16. Model for superconductor-metal tunneling with applied voltages of (a) $V=0$, (b) $V=\Delta/e$ and (c) $V=-\Delta/e$. Occupied states are cross-hatched below Fermi energy. SIS tunneling current grows when (d) $V\geq 2\Delta/e$. \circ denotes Cooper pair and \bullet normal electron.

When superelectron pairs tunnel together, further effects occur. These effects, first predicted by Josephson, occur typically in a circuit containing weak links. The weak links can be SIS junctions, cracks, grain boundaries, point contacts, linear contacts, material constructions or other inhomogeneities. The Josephson effect results from interference between macroscopic waves of superconducting current. If a current is generated across a weak link, the superconducting waves are coherent, but differ by some phase shift dependent on the barrier. There are two principal phenomena: the dc effect and ac effect (Bourdillon & Bourdillon, 1994).

a) Josephson dc effect

A dc current will flow across a weak link in the absence of any electric or magnetic field. The current of superconducting pairs across the weak link, connected to an electrical circuit as in Figure 1.17.a, is related to the phase difference, $\Delta\theta$, of supercurrents on either side of the junction. The current can be written

$$I = I_0 \sin \Delta\theta \quad (1.20)$$

where I_0 is characteristic of the junction. With zero applied voltage the current can have any value between $+I_0$ and $-I_0$.

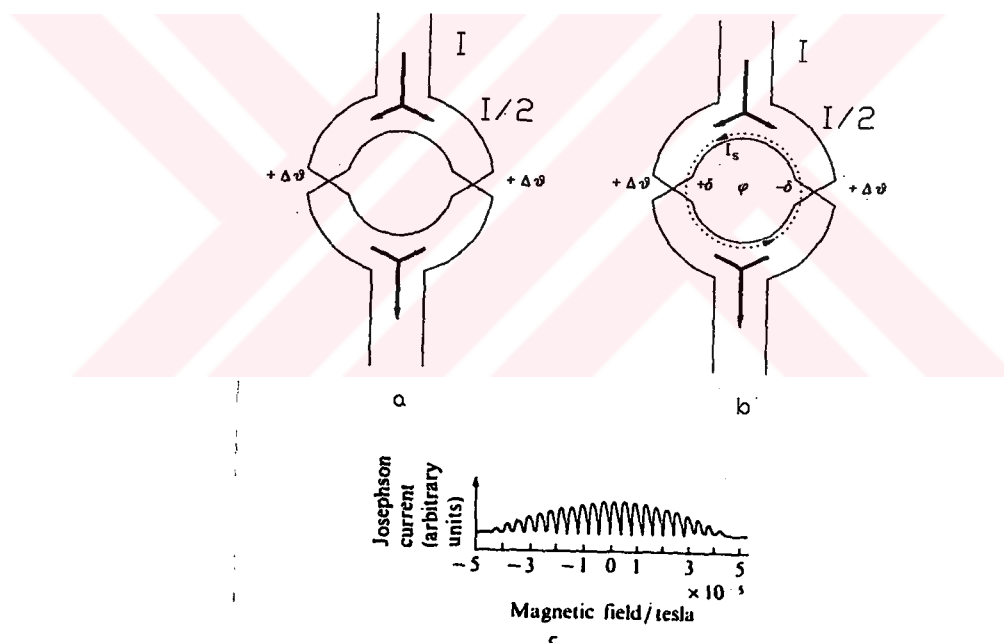


Figure 1.17. (a) Supercurrent dividing through two weak links suffers phase change $\Delta\theta$ due to applied potential. (b) Magnetic flux induces additional circulating supercurrent, which suffers phase changes $+\delta$ and $-\delta$ at the junctions. (c) Measurement of the resulting supercurrent in a low T_c SQUID interferometer shows interference in current transport.

b) Josephson ac effect

If a dc voltage is applied across a junction, radio frequency current oscillations result. Further, if a radio voltage is also applied, a dc current can be produced. If a dc voltage, V , is applied, the current at time t becomes I with oscillating frequency ω

$$I = I_0 \sin \Delta\theta(t) = I_0 \sin \{ \Delta\theta(0) - 2eVt/\hbar \} \quad (1.21)$$

$$\omega = 2eV/\hbar \quad (1.22)$$

Josephson currents can be made to interfere in a SQUID (superconducting quantum interference device). This consists of a circuit with two (Fig.1.17.b; Bordillon&Bourdillon, 1994) or more Josephson junctions. The loop shown is connected to a current supply and passing a current less than $2I_0$. The weak links can be identical so that half of the current flows through each link with a phase change $\Delta\theta$. If a magnetic field, \mathbf{B} , is now applied, a persistent current, I_s , will be induced round the loop. This will add δ to the phase change, $\Delta\theta$ at one junction, and subtract from the other. The two currents can be written

$$I/2 + I_s = I_0 \sin (\Delta\theta + \delta) \quad (1.23-a)$$

$$I/2 - I_s = I_0 \sin (\Delta\theta - \delta) \quad (1.23-b)$$

The total current is still I , but this now defined through a trigonometric addition of the preceding two equations:

$$I = 2I_0 \cos \delta \sin \Delta\theta \quad (1.24)$$

Each flux quantum produces a phase change of 2π , so that for each junction $\delta = n\pi$, where n is the number of flux quanta in \mathbf{B} . Since

$$n\Phi_0 = \int \mathbf{B} \cdot d\mathbf{S} \quad (1.25)$$

integrated over the area, S , of the loop, it follows

$$I = 2I_0 |\cos(n\pi)| \sin \Delta\theta \quad (1.26)$$

The maximum current depends on the flux in the loop, and the period is one flux quantum (Fig 1.17.c). The SQUID magnetometer is the most sensitive detector of magnetic flux.

1. 2. 3. High Temperature Superconductors

There are some characteristic features in the structures of the high- T_c superconductive oxides. The first one is that the species of component elements are many in number, at least four. The second one is that the crystal structures are of new types named as perovskite. They seem to be rather complicated, but there is a common structural element, a CuO_2 plane, in which the superconductive current runs. Atomic planes of the remaining part, sandwiching the CuO_2 plane, also play an important role in that they accommodate additional oxygen atoms or defects to provide carriers (positive holes in the case of Bi-based superconductors) to the CuO_2 planes. They are then called the charged reservoir. The transition temperature between superconductive and nonsuperconductive states, T_c , strongly depends on the concentration of carriers in the CuO_2 planes, which closely relates to structures in the charge reservoirs and the number of CuO_2 planes.

The third characteristic structural feature is that the high- T_c superconductors often include various kinds of lattice imperfections and impurity phases, which are nonsuperconductive. They constitute a variety of microstructures, strongly affecting the critical current density, J_c , because they closely relate to the weak link at boundaries between superconductive grains as well as to the pinning of magnetic fluxoids. These defects depend on processing conditions. For example, intergranular phases result from inhomogeneous mixing of starting powders and from impurities. Some inhomogeneity results from thermodynamic disorder.

The common feature of these ceramic materials is also positively charged hole carriers. Hall measurement provide generally the most reliable measurements of carrier densities, varied with oxygen concentration, in the various HTSC which have positive values of R_h .

1. 2. 3. 1. Crystal Structure

After the discovery of the superconductivity in $\text{Bi}_2\text{Sr}_2\text{Cu}_2\text{O}_{7-\delta}$ by Michael et al. at 1987 at 22 K, in 1988 Maeda et al. reported that the addition of Ca in Bi-Sr-Cu-O

system has been raised the critical temperature to 105 K. A key point in attaining high T_c in the Bi oxides is the coexistence of two kinds of alkaline earth elements, Sr and Ca. The Ca ion enables the CuO_2 layers to be stacked up, which is responsible for the increase of T_c (Maeda & Togano, 1996).

The phases of Bi-based superconductors are generally formulated by $\text{Bi}_2\text{Sr}_2\text{Ca}_{n-1}\text{Cu}_n\text{O}_{2n+4+x}$. It is known that three phases, $\text{Bi}_2\text{Sr}_2\text{CuO}_{6+x}$ ($n=1$, 2201 phase), $\text{Bi}_2\text{Sr}_2\text{CaCu}_2\text{O}_{8+x}$ ($n=2$, 2212 phase) and $\text{Bi}_2\text{Sr}_2\text{Ca}_2\text{Cu}_3\text{O}_{10+x}$ ($n=3$, 2223 phase), are formed by a conventional sintering method. These homologous phases are often intergrown to each other; it is difficult to prepare any of these as a complete monophasic, especially 2223 phase. The substitution of cations frequently occurs in these phases. It affects their stability and plays an essential role especially in the formation of the 2201 phase.

1. 2. 3. 1. 1. Crystal Structure of $\text{Bi}_2\text{Sr}_2\text{CuO}_{6+x}$

The first member of the BSCCO system (representation of $\text{Bi}_2\text{Sr}_2\text{Ca}_{n-1}\text{Cu}_n\text{O}_{2n+4+x}$ in literature) has a minimum critical temperature, $T_c \leq 20$ K. For the phase the simplest stacking sequence of atom planes may be shown by



Crystal structure of phase contains a square pyramidal Cu layers, which are sandwiched between two SrO layers. In Bi_2O_2 layer, Bi is in distorted octahedral structure. The lattice parameters are $a = 3,81\sqrt{2} \approx 5,39 \text{ \AA}$ and $c = 24,6 \text{ \AA}$. BiO layers are at the bottom of crystal structure (Figure 1.18; Nezir,1996) and Cu atoms are in connection with 6 oxygen atoms in regular octahedral structure (Maeda & Togano,1996).

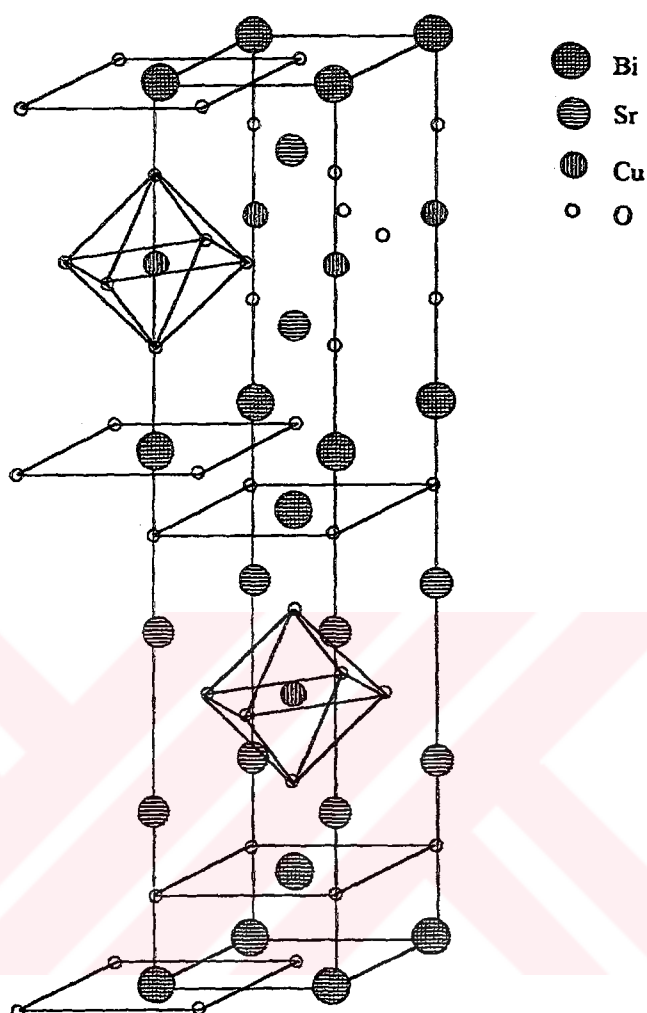


Figure 1.18. Crystal structure of $\text{Bi}_2\text{Sr}_2\text{CuO}_6$ system.

1.2.3.1.2. Crystal Structure of $\text{Bi}_2\text{Sr}_2\text{CaCu}_2\text{O}_{8+x}$

The second member of the BSCCO (representation of $\text{Bi}_2\text{Sr}_2\text{Ca}_{n-1}\text{Cu}_n\text{O}_{2n+4+x}$ in literature) has a critical temperature $T_c = 85$ K. The structure has a pseudotetragonal symmetry with lattice parameters $a = b = 5,4$ Å and $c = 30,7$ Å. Figure 1.19.a is a model for the fundamental unit cell of the 2212 phase (Nezir, 1996). It contains four formula units and is simply denoted by a stacking of atomic planes in the sequence of



Furthermore, these planes can be divided into two kinds of layers. One is a layer consisting of SrO/CuO₂/Ca/CuO₂/SrO, which has a structure of perovskite type. The CuO₂ planes function as the conduction planes of superconductive current. Another is a SrO/(BiO)₂/SrO layer, which has a structure of NaCl type. The (BiO)₂ planes contribute as a charge reservoir. In contrast to 2201 phase structure, in 2212 phase Cu atoms are connecting with 5 oxygen atoms in pyramid shape. Between these pyramids, there is Ca atom, which hasn't oxygen at a-b plane.

1. 2. 3. 1. 3. Crystal Structure of Bi₂Sr₂Ca₂Cu₃O_{10+x}

The critical temperature of Bi₂Sr₂Ca₂Cu₃O_{10+x} (2223) phase is 110 K when doped with Pb. This phase has a tetragonal structure. In addition to two BiO and SrO layers, there is two Ca and three CuO layers, which increase c-axis parameter to 37,1 Å. As shown in Figure 1.19.b, three CuO layer are separated from each other by Ca planes. The two Cu ions have pyramidal coordination, while the third is square planar.

1. 2. 3. 2. Characterization

The two most characteristic properties displayed by superconductors are zero resistance and expulsion of applied magnetic field. Ambiguities and experimental artifacts can occur in each of these individual measurements, so the identification of superconductivity in a new compound requires, not just careful experimentation, but also the measurement of both transport and magnetic phenomena. The critical temperature of superconducting material is usually determined by resistivity, a.c. susceptibility, d.c. magnetization (zero field cooled), the Meissner effect (field cooled) or specific heat discontinuity measurements.

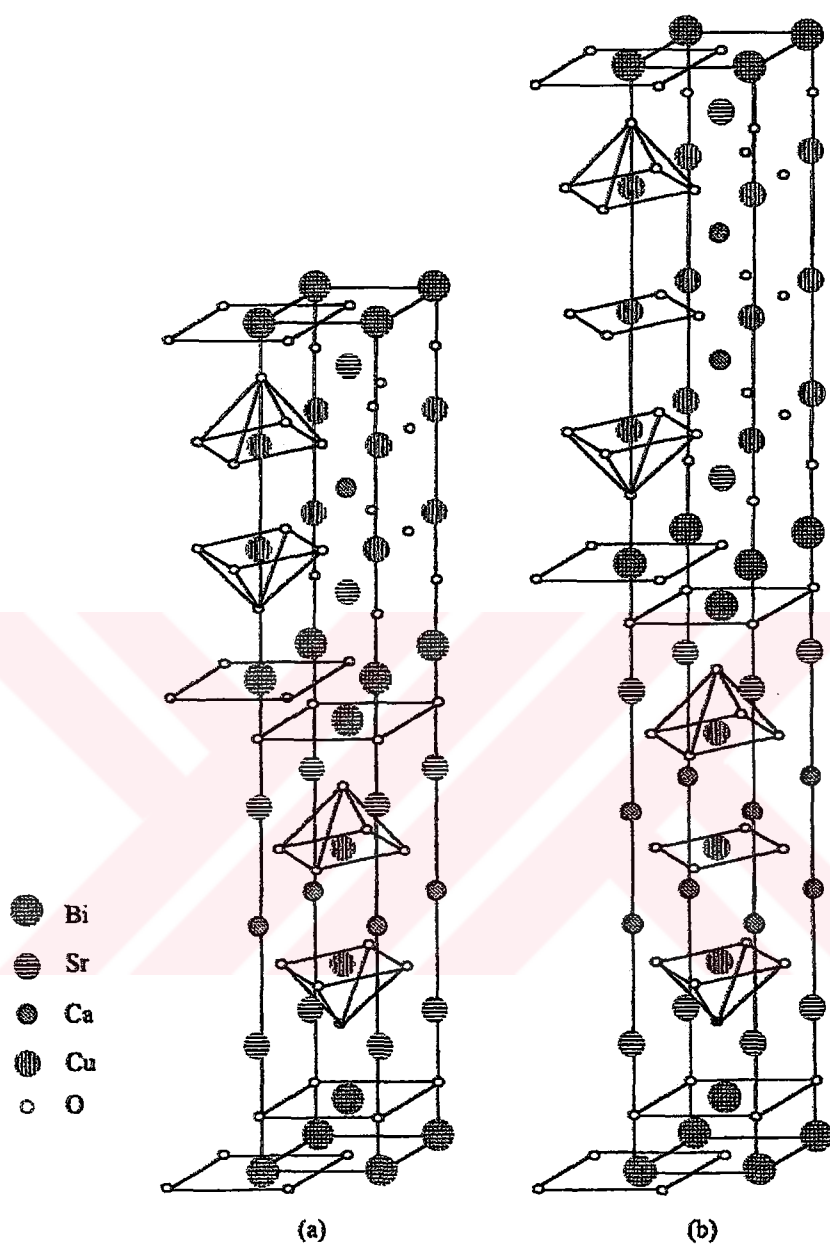


Figure 1.19. Crystal structure of (a) $\text{Bi}_2\text{Sr}_2\text{CaCu}_2\text{O}_8$ and (b) $\text{Bi}_2\text{Sr}_2\text{Ca}_2\text{Cu}_3\text{O}_{10}$ systems.

1. 2. 3. 2. 1. Electrical properties

Resistivity and magnetic properties are both used for measuring T_c . However, since the critical temperature, $T_c(B, I)$, depends on both applied field and on current. $T_c(0,0)$ can only be measured approximately at low field and low current. Curve of the type shown in Figure 1.1. was obtained from measurements by the four-probe technique with the smallest supply currents needed to detect the transitional voltage drop. A typical current is 1 mA. At temperatures below T_c , the resistivity of the superconductor becomes very small: values less than $10^{-23} \Omega\cdot\text{cm}$, have been measured in conventional low temperature superconductors by persistent currents. With increasing currents, especially in the high temperature superconductors, the resistivity is complicated by significant resistive flux flow, especially as $T \rightarrow T_c$. This residual resistance is due not only to the comparatively high thermal energies at these temperatures, but also to the small coherence lengths which imply comparatively small flux pinning forces. Therefore the measurements of *zero resistance* requires definition concerning what exactly to be measured. Zero resistance is sometimes defined as a resistivity less than that of Cu at the same temperature, $\sim 10^{-8} \Omega\cdot\text{cm}$.

1. 2. 3. 2. 2. Crystal Structures

The ready accessibility of X-ray diffraction makes it useful as a technique, not only for phase identification, but more basically for initial identification of lattice structure and for modelling of the basic unit cell. With a knowledge of the chemical composition of a solid and of ionic sizes, structural models can be built and used in refinement procedures with either X-ray or neutron diffraction spectra. In sheet textured material, diffraction is enhanced for peaks corresponding to crystal planes lying parallel to the sheet surface. Diffraction patterns for 2201, 2212 and 2223 phases of Bi-based system with CuK_α radiation is shown in Figure 1.20(Nezir,1996).

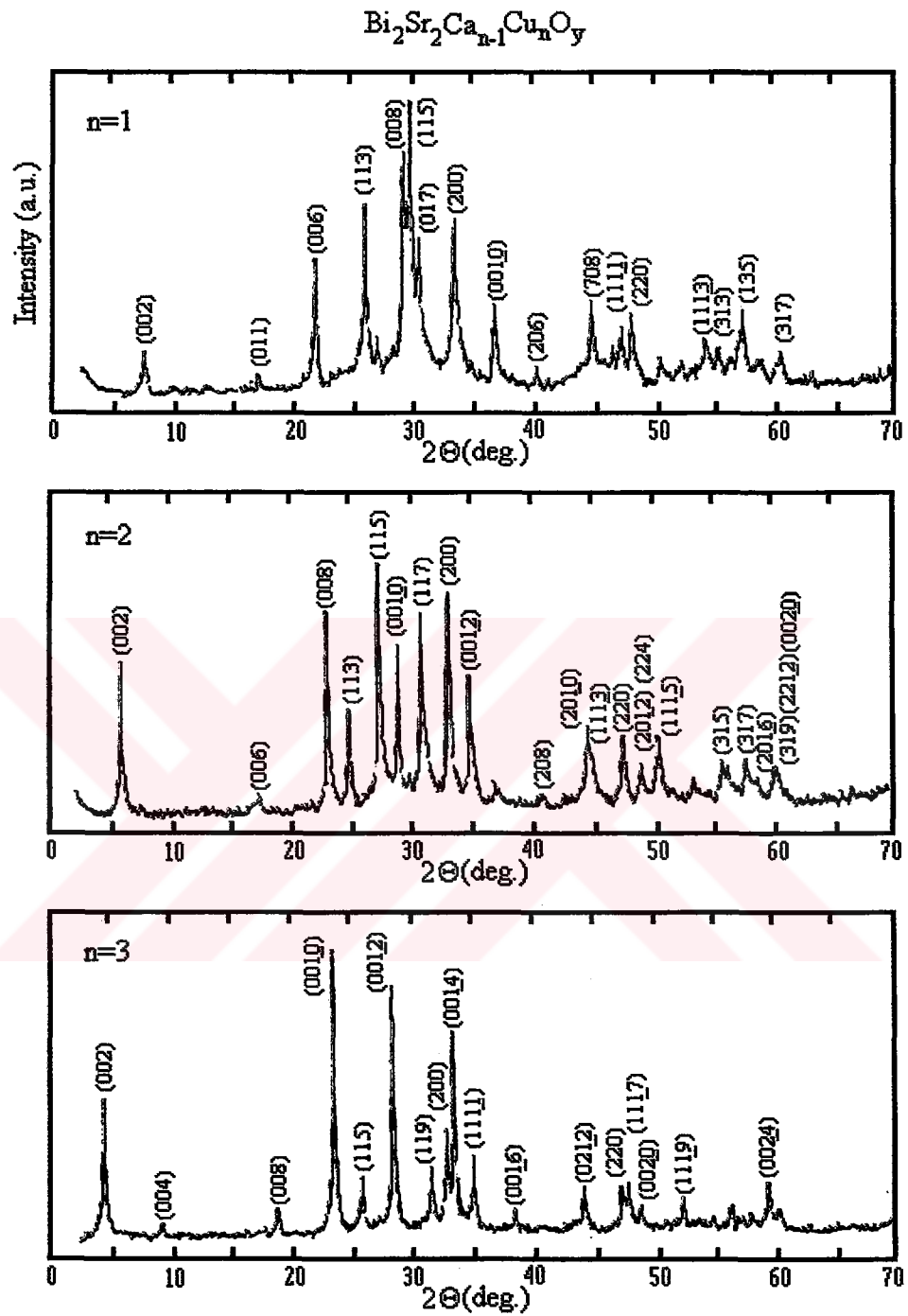


Figure 1.20. Powder X-ray diffraction patterns ($\text{CuK}\alpha$) of single phase BSCCO system. [$n=1$ (2201); $n=2$ (2212); $n=3$ (2223)]

1. 2. 3. 2. 3. Microstructures

After chemical reaction, texture, i.e., the orientation of microcrystalline grains relative to material geometry, is the feature which provides the greatest control in optimizing current transport and magnetic properties in bulk high temperature superconductors. Microstructures are observed in variety of ways, and each other technique bears its own merits. SEM (scanning electron microscopy) is the workhorse of microstructural characterisation. This is because of the variety of signals that can be recorded, each providing its own peculiar information, including elemental analysis by energy-dispersive X-ray spectroscopy (EDX). The two signals most commonly used in SEM imaging are the secondary electron signal and the backscattered signal. The secondary electrons are of low energy, 0-10 eV, emitted from the surface of a specimen, scanned by the focused electron beam, accelerated by a potential between 5-40 kV.

The secondary electron image is often affected by artifacts on the specimen surface, including surface corrosion and surface topography, especially on fractured specimens. This is because the secondary electrons exit from a shallow depth owing their low energies. They are therefore sensitive to surface phenomena, and secondary electron images provide comparatively high spatial resolution because most emission originates close to the point of incidence of the focused probe.

CHAPTER TWO

EXPERIMENTAL DETAILS

2. 1. Preparation of Samples

The chemical reactions which are used to form ceramic compounds follow after the processing of starting powders. The preparation of the powders constitute the most critical features, after temperature and time control, to the formation of homogeneous final reaction products. Powder processing involves the control both of particle size and of mixing of powders, whether starting powders or partly reacted powders. Generally the chemical reactions are diffusion limited, and they can be speeded up by prior production of fine, well mixed particles.

A solid-state reaction method is a general method producing superconducting oxide. Figure 2.1. shows the flowchart for the solid-state process forming calcsined powder. Because the superconductivity of oxide is significantly influenced by the minute deviation of the molar ratio of composed molecules, particular attention should be given to the correct mixing ratio of raw material powders with high purity.

Prior to reacting, these powders are broken by mixing with other compounds so that neighbouring grains react in a furnace to form new stable phases. These initial decomposition of stable starting powders, by heating below their melting points, is known as *calsination*. The rate at which calsination occurs depends on (1) the rate of reaction at the reacting surface, (2) the rate of heat transfer and (3) the rate of gas transport. The powders to be calcsined are not normally pressed. Extra porosity is often produced by escaping gases, and the reactions do not go to completion partly

owing to small contact areas at interface between grains. Repeated mixing, pressing and grinding are needed to make a reaction go to completion so as to form single phase high- T_c compounds and to form a homogeneous sintered product. Surface contact between particles is maximized by pressing the powders before sintering, and the initial shape of the compacted material can often be retained, with more or less shrinkage or expansion, depending on processing conditions.

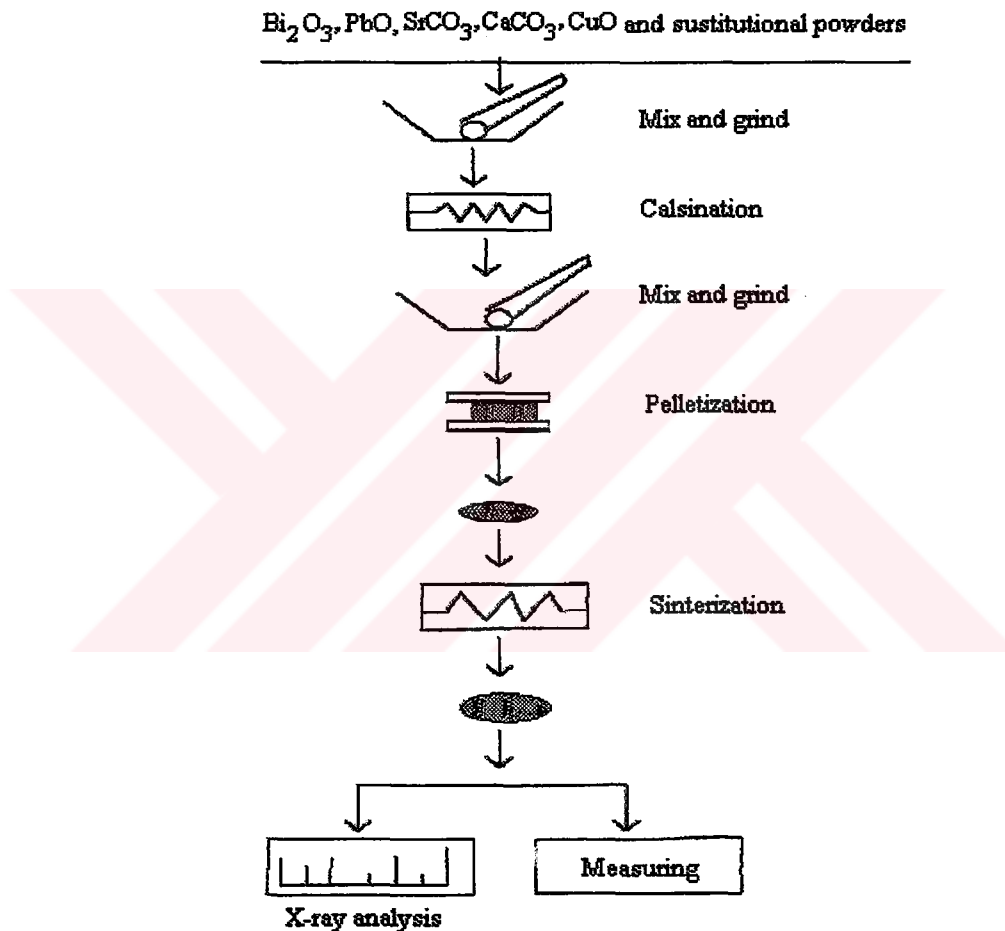


Figure 2.1. Solid-state reaction method procedure for producing BPSCCO.

The dominant physical factor controlling sintering is temperature. After calcination process prepared powders are shaping in pellets to ensure large areas of surface contact between grains. Pellets are most easily formed by axial pressure applied with a hydraulic press to powder in die. The effects of pressure are (1) to reduce pore size,

(2) to break up particles especially at surface in contact, and (3) to introduce strain and plastic flow.

2.2. Characterization of Samples

2.2.1. Resistivity Measurements

The dc resistivity of a sample is measured by the voltage drop across it, when a current of known magnitude passes. The terminals used for measuring the voltage pass little current when connected to a high impedance voltmeter. These terminals are distinct from those used for passing the main part of the current through the specimen, whose voltage drops in both leads and contacts are significant.

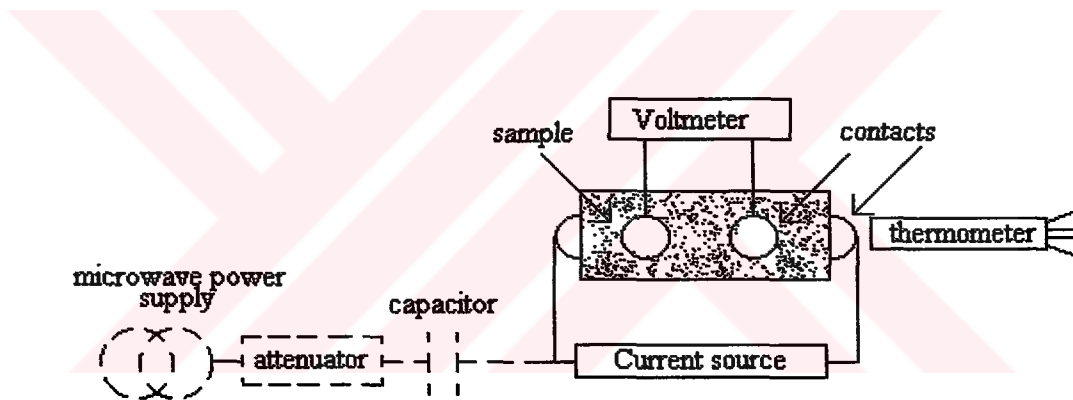


Figure 2.2. Schematic four-probe resistance apparatus with temperature sensor used for measuring dc resistivity.

Figure 2.2. shows a schematic diagram of four probes connected to a sample whose temperature is measured by a temperature sensor in thermal contact with the specimen. The fabrication of low resistance ohmic electrical contacts is important not only to characterisation, but also to device fabrication. We have used copper wires at 0.05 mm in diameter and silver paste to get contacts with a little resistance.

A cryogenic arrangement is shown in Figure 2.3. Cooling occurs by immersing the sample into a cryogenic liquid, e.g., nitrogen, or into the cold gas above the cryogenic liquid. The thermal gradients inside the dewar can be used to roughly regulate the temperature. The thermal shield is used to maintain uniform temperature around the specimen and temperature sensor. For high uniformity, the shield and specimen support block are made of OFHC (oxygen-free high conductivity copper) and supported by thin walled low conductivity stainless steel tube.

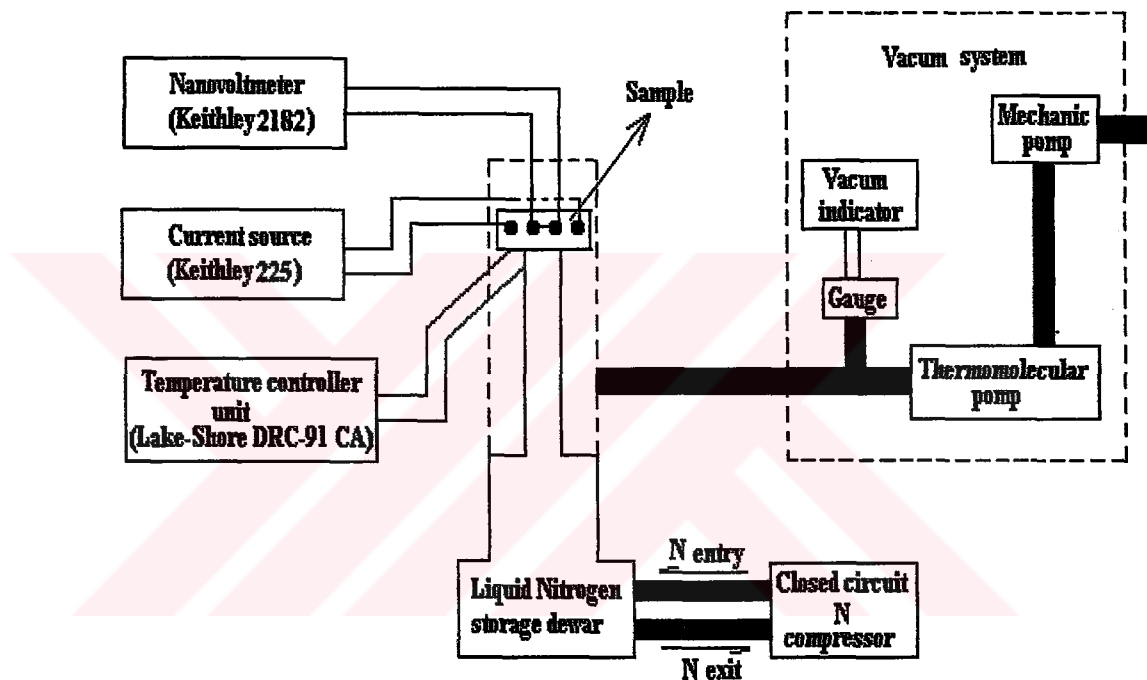


Figure 2.3. Cryogenic system for the measurement of resistivity.

2. 2. 2. X-Ray Diffraction Measurements

X-rays, arising when matter is irradiated with a beam of high-energy charged particles, are relatively short wavelength and high-energy beams of electromagnetic radiation. High temperature superconductors are polycrystalline materials and an ideal polycrystalline material or powder is an ensemble of a very large number of randomly oriented crystallites. X-ray diffraction is used for identification of compounds by their diffraction patterns. There are essentially three methods: The

rotating crystal method, the Laue method and the powder method. Regardless of the method used, the quantities measured are essentially the same.

1. The scattering angle 2Θ between the diffracted and incident beams. By substituting $\sin\Theta$ into Bragg's law ($2d \sin\Theta = n\lambda$), one determines the interplanar spacing as well as the orientation of the plane responsible for the diffraction.
2. The intensity I of the diffracted beam. This quantity determines the cell-structure factor, F_{hkl} , and hence gives information concerning the arrangement of atoms in the unit cell.

The powder diffraction method is used to determine the crystal structure even if the specimen is not a single crystal. The sample may be made up of fine, grained powder packed into a cylindrical glass tube, or it may be polycrystalline, in which case it is made up of large number of small crystallites oriented more or less randomly. A monochromatic beam impinges on the specimen, and the diffracted beams are recorded on a cylindrical film surrounding it.

Because of the large number of crystallites which are randomly oriented, there is always enough of these which have the proper orientation relative to the incident monochromatic beam to satisfy Bragg's law, and hence a diffracted beam emerges at the corresponding angle. Since both Θ and λ are measurable, one can determine the interplanar spacing (Jenkins & Snyder, 1996).

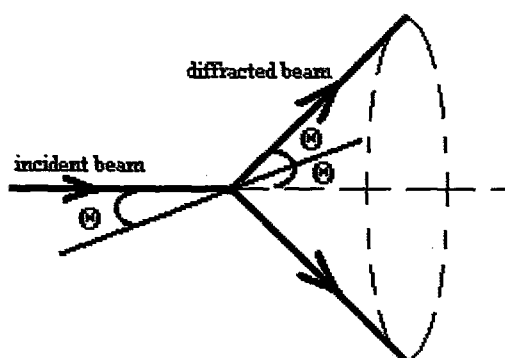


Figure 2.4. Schematic illustration of the formation of a cone of diffracted radiation from a given lattice plane in the powder diffraction method.

Other sets of planes lead to other diffracted beams corresponding to different planar spacing for the same wavelength. Thus one can actually determine the lattice parameters quite accurately, particularly if the crystal structure are already known. Since the specimen is symmetric under rotation around the incident beam as an axis, the diffracted beam corresponding to each scattering angle 2θ fans out along a cone whose axis lies along the incident beam as shown in Figure 2.4.

X-ray diffraction patterns of ZnO substituted samples were obtained at Dokuz Eylül University, İzmir, Mining Engineering Department by using JEOL JSDX 100S Diffractometer in the $2\theta=3^\circ-60^\circ$ range with CuK_α radiation, 30 kV accelerating potential and 22 mA current with powder diffraction method. Diffraction patterns of Ag_2O substituted samples were obtained at Cumhuriyet University, Sivas, Geology Engineering Department in the $2\theta=0^\circ-55^\circ$ range CuK_α radiation by a Rigaku D.Max 3C XRD.

2. 2. 3. Scanning Electron Microscopy (SEM) Measurements

SEM uses the secondary electrons that are ejected from a sample to image a surface. These images are useful for studying surface morphology or measuring particle sizes. The electron beam is rastered across the sample by ramping the voltages on X and Y deflection plates through which the electron beam passes (the Z-axis is the electron beam direction). A detector above the sample detects the secondary electrons to produce an intensity map as a function of electron beam position, which is displayed on a video or computer screen.

The SEM microphotographs of the microstructure were taken by using JEOL JXA733 microscope at Dokuz Eylül University, İzmir, Mining Engineering Department.

2. 3. Effects of Substitution and Doping in BSCCO System

2. 3. 1. Formation of Bi-2223 Phase

High-temperature superconductors are very interesting and also challenging. One of the most widely studied systems is the Bi-Sr-Ca-Cu-O system, owing to its chemical stability against aggressive environmental contaminations (for example water vapour and CO₂) compared to the La-Sr-Cu-O or Y-Ba-Cu-O systems, which has made it attractive for potential applications.

High-T_c phase can be formed by the diffusion of Ca, Cu and O atoms into low-T_c phase. However, it is widely accepted that the diffusion of Ca and Cu is very slow and therefore requires prolonged heat treatments (Padam et al., 1991). Prolonged heating results in problems of reproducibility and control over stoichiometry. Yet two major issues, namely the kinetics and the stability of the phase, seem to complicate the development of single-phase 2223 superconductors (Khan & Kayani, 1998). The 2223 phase is stable only in a very narrow temperature range and the kinetics of its formation is so slow that it is almost impossible to obtain a pure 2223 phase.

Suzuki et al. (Suzuki, Inoue & Hayashi, 1989) reported that T_c for the low-T_c phase gradually increased from 85 to 97 K with sintering time, while other researchers have reported the values are in 75-85 K range. The reasons for the variety of T_c values are not clear at present.

It has been reported that partial substitution of Bismuth by Lead plays an important role not only in stabilizing the high-T_c phase by suppressing the low-T_c 2212 one, but also enhances the values of both T_c as well as density without affecting the structural properties of Bi-2212 (Anis-Ur-Rehman et al., 1998; Ravinder Reddy et al., 1995; Kocabaş, 1994). In fact, it has also been reported that the addition of Pb up to a concentration of 0,35 mol % slightly improves the T_c and density values without affecting structure crystallographically (Ravinder Reddy et al., 1995).

All the proposed (Bi,Pb)-2223 formation mechanisms accept that a liquid phase related to Ca_2PbO_4 is present (Yavuz et al., 1998). The addition of Pb, combined with excess Ca, leads to the formation of Ca_2PbO_4 , which acts as a reservoir for Ca and prevents PbO from acting as a flux. The formation of the Ca_2PbO_4 phase produces partially melted materials (non-superconducting phases such as Ca_2CuO_3 and $\text{Sr}_{14}\text{Cu}_{24}\text{O}_{41}$), offers a fast reaction path to form 2223, and accelerates the formation of 2212 phase. Ca_2PbO_4 decomposes or melts around at 825°C in the presence of 2212 phase reported that Ca_2PbO_4 by itself is stable (up to 980°C in air), and widens and lowers the temperature range of partial melting. The rate of formation of 2223 depends on the atmosphere under which annealing occurs and on doping.

2. 3. 2. Effect of Dopant and Substitution

In high-temperature superconductors, understanding the role of substituents and dopants is of great importance for scientific as well as applied purposes. When doping, the following aspects are generally under consideration:

- Change in electron / hole concentration or other physical parameters. The hole concentration in high- T_c superconductors may be changed by replacement of atoms, by change of oxygen contents and oxygen redistribution (Romanenko et al., 2000).
- Enhancement of the desired phase formation and phase stability. The multiplicity of phases in BPSCCO system is a major problem in synthesis of homogeneous material.
- Improvement of the superconducting characteristics. (e.g., formation of effective pinning centers leading to critical current increase)

The influence of the dopants on synthesis processes and on final superconducting characteristics could depend on the type and phase content of the precursor powders, technological method/route and the type of the dopant (Badica, Aldica & Mandache, 2000).

2. 3. 2. 1. Effect of Zn

There is an intense debate in the literature concerning the origin of the detrimental effect on Zn on critical temperature in high-temperature superconductors. The substitution of Zn in YBCO (123), BSCCO and HgBaCuO superconducting systems depresses T_c at a rather dramatic rate in fully oxygenated compounds (Li et al.,1999; Bichhle et al., 1991; Halim et al. ,1999; Tepe & Abukay, 1997; Hu et al., 2000) with the rate being in the oxygen deficient samples.

The transition width increases for high Zn contents. The larger transition width comes from inhomogeneity due to the Zn substitution for Cu (Park et al., 1999) which leads to a redistribution of charge on several sites nearby (Gupta & Gupta, 1998).

The deteriorative of zinc doping on superconductivity mainly originates from the strong and extended perturbation caused by Zn^{2+} . First, Zn^{2+} redistributes the charge on neighbouring atomic sites and produces a considerable number of scattering centers that break the Cooper pairs. Second, Zn^{2+} modifies the spatial location and electronic state of apical oxygen and affects the interlayer charge transfer, thus strongly suppressing the superconductivity (Abd-Shukor & Lo, 2001).

2. 3. 3. 2. Effect of Ag

The beneficial and detrimental effects of Ag addition in (Bi,Pb)-Sr-Ca-Cu-O system have been studied by several groups. Ag is known to promote the formation of 2223 phase and improve c-axis texture, mechanical ductility and critical current (Chiu et al., 1994; Sobha et al., 1998).

However, the published results of silver effect on superconductivity of BPSCCO compound are very inconsistent. For instance, some researchers reported that additions depressed the critical temperature of Bi-2223 bulk samples (Kocabaş &

Kazancı, 1996; Kocabaş et al., 2000), while others (Guo, Liu & Dou, 1994; Khan, Kayani & ul Haq, 1997; Muralidhar et al., 1994; Muralidhar et al., 1992) claimed that silver caused no change in T_c for the same material. Investigations of some researchers working on Ag affect, however, showed an increase in T_c for samples with silver contents up to certain volume and then a decrease with more silver (Matsushita et al., 1994; Yu et al., 1997; Cömert et al., 1994).

Conflicting results have also been reported about the influence of silver on critical density and J_c behaviour in magnetic fields. Therefore, further detailed investigation is needed to understand the behaviour of silver in BPSCCO superconductors.



CHAPTER THREE

EXPERIMENTAL RESULTS

3. 1. Experimental Procedure of Preparation of Samples

The ceramic superconducting samples of $\text{Bi}_{1.7}\text{Pb}_{0.3}\text{Sr}_2\text{Ca}_{2-x}\text{M}_x\text{Cu}_3\text{O}_y$ ($\text{M} = \text{Zn}$ and Ag) system were prepared from appropriate mixtures of high purity Bi_2O_3 (%99.99 Aldrich Co.), PbO (%99.999 Aldrich Co.), SrCO_3 (%99.9 Merck Co.), CaCO_3 (%99.9 Merck Co.), CuO (%99.99 Aldrich Co.), ZnO (%99.99 Aldrich Co.) and Ag_2O (%99.9 Aldrich Co.) by standard solid state reaction method shown in Figure 3.1.

The substitution ratios of Ca by ZnO and Ag_2O are in $x = 0.00 - 0.20$ range. Starting component powders first have been weighted in cationic ratios with ± 0.0001 g sensitivity Scaltec balance. After weighting, powders were mixed and well grounded at five different ratios by naming A ($x = 0.00$), B ($x = 0.05$), C ($x = 0.10$), D ($x = 0.15$) and E ($x = 0.20$). These mixtures were heat-treated twice at 800°C for 30 hours in alumina crucibles. The heat-treated powders were grounded again in a mortar with a pestle and were uniaxially pressed at 375 MPa pressure. Prepared pellets were 13 mm in diameter and 1-1.5 mm thick. These pellets were sintered at 850°C for 250 hours by using $7^\circ\text{C}/\text{minute}$ heating rate and furnace cooled down to room temperature.

In this study we have used Nabertherm furnace for heating processes which could heat up to 1200°C . The temperature variation from the center of furnace is $\pm 1^\circ\text{C}$ so we were able to heat more than one samples. Furnace can be controlled automatically by adjusting desired heating ratio.

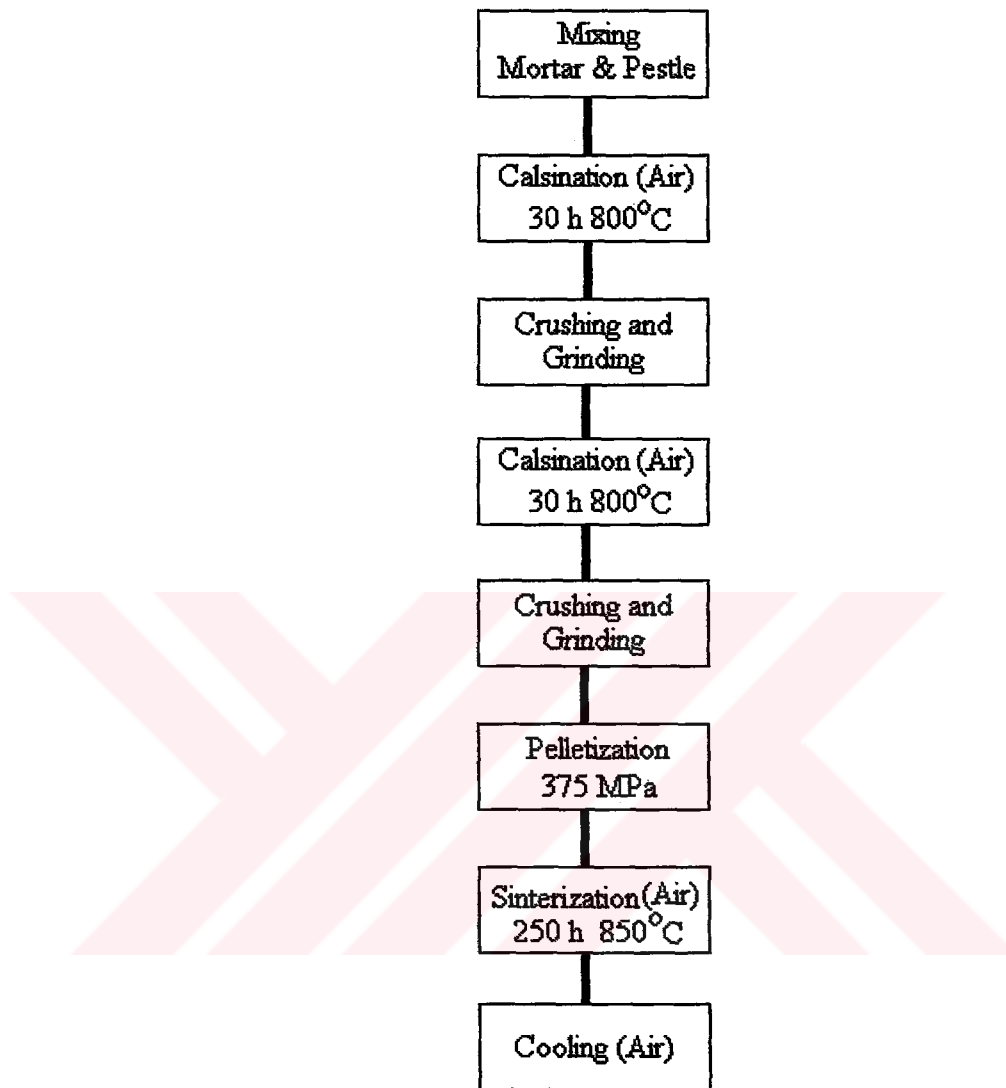


Figure 3.1. Flowchart of the solid-state reaction method.

3. 2. Effect of Zinc oxide Substitution

3. 2. 1. Resistivity Measurements

The temperature dependence of resistance of all samples is shown in Figure 3.2 in $T = 80\text{-}220$ K range. All samples display a metallic character above onset temperature, which is defined as the temperature where resistance-temperature plot

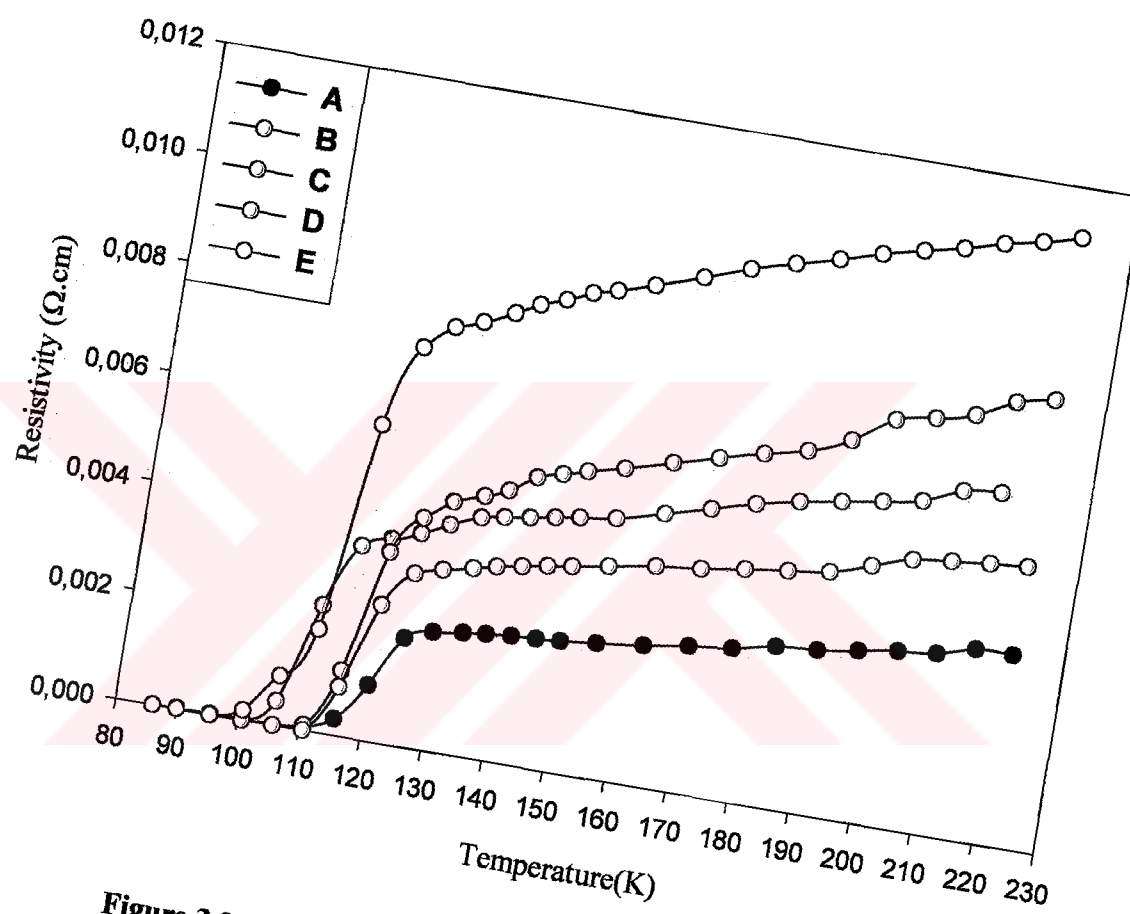


Figure 3.2. Resistivity versus temperature of ZnO substituted samples.
A ($x=0.00$), B ($x=0.05$), C ($x=0.10$), D ($x=0.15$), E ($x=0.20$)

deviates from linearity. The onset temperature of samples is 125 K, 115 K, 123 K, 121 K and 118 K respectively. It's evident that for the highest substitution ratio, resistivity was strongly increased in metallic character region. The critical temperature, zero resistance temperature, is 105 K, 100 K, 108 K, 110 K and 95 K respectively. The resistance drop occurred in a single step implying that the samples are mainly of single phase. Pb doped BSCCO (2223) system has 110 K offset temperature. Results obtained from four-probe point resistivity measurements are nearly to this value. The most convenient values are for C ($x=0.10$) and D ($x=0.15$) samples and so it's possible to say that up to certain substitution ratio, ZnO improves the formation of high- T_c phase. Transition width, which is a parameter for the purity of samples, is respectively 20 K, 15 K, 15 K, 11 K and 23 K. This indicates that the narrowest transition width for samples B, C and D is in agreement with T_c values. However, the highest substitution ratio ($x=0.20$) has broadened the width of the transition temperature implying the increasing of the weak links. The results obtained by Halim et al. (Halim et al., 1999) for T_c , in $\text{Bi}_2\text{Pb}_{0.6}\text{Sr}_2\text{Ca}_2\text{Cu}_3\text{O}_8$ composition, indicate that zero resistance value decreases with zinc substitution up to 75 K. They also reported that the coupling of the grains in Zn doped sample ($x=0.10$ and $x=0.02$) are weaker than that of Ba doped samples. Tepe et al. (Tepe & Abukay, 1997) found that T_c decreases with increasing x up to 0.20 from 104.5 K to 90.30 K in $\text{Bi}_{1.7}\text{Pb}_{0.3}\text{Sr}_2\text{Ca}_2\text{Zn}_x\text{Cu}_{3-x}\text{O}_y$ system. In contrary to the results given in literature in our study we found that up to certain value of ZnO substitution, critical temperature increases. This may be due to the different starting compositions and different annealing conditions.

3. 2. 2. X-ray Diffraction Measurements

The powder XRD patterns of all samples are given in Figure 3.3. The high- T_c and low- T_c phase peaks were identified by using the tables given by Bansal et.al. and Pandey et.al.(Appendix B). All samples have a multiphase nature with high and low- T_c peaks along with ZnO and CuO impurity phases, which indicates the difficulty in obtaining a single phase material by the conventional ceramic method. Peaks

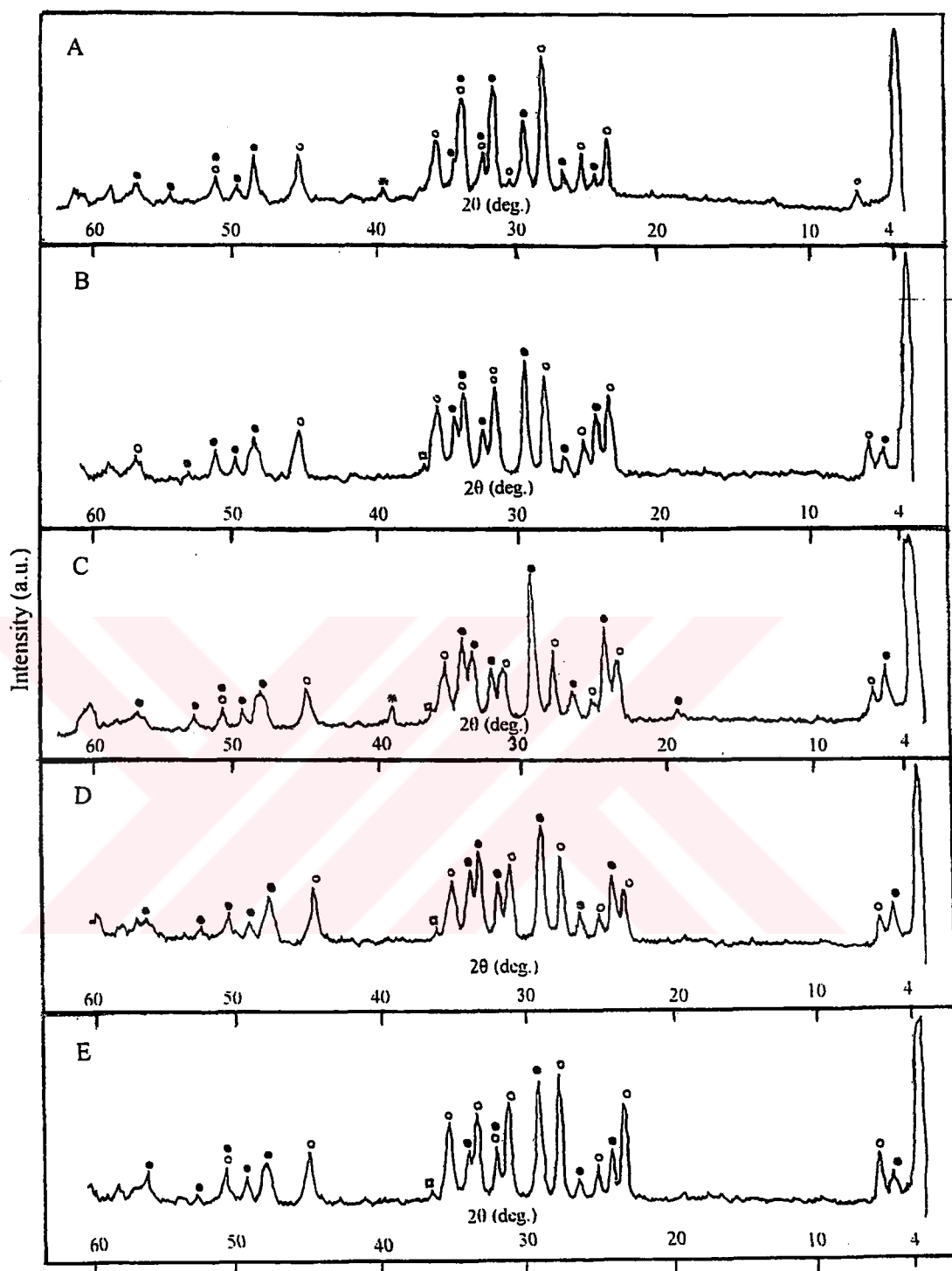


Figure 3.3. XRD patterns of ZnO substituted samples of $\text{Bi}_{1.7}\text{Pb}_{0.3}\text{Sr}_2\text{Ca}_{2-x}\text{Zn}_x\text{Cu}_3\text{O}_y$ system. [A($x=0.00$), B($x=0.05$), C($x=0.10$), D($x=0.15$), E($x=0.20$)]
 ○- Low- T_c phase; ●-High- T_c phase; □-ZnO; *- CuO

corresponding to $2\theta = 4.7^\circ$ and $2\theta = 5.7^\circ$, named as H(002) and L(002) are showing in all samples with different intensities. The intensity of H(002) has maximum values for samples C and D, in contrary to the peak intensity for L(002) which has minimum value for this samples. The most visible peaks which can be seen in $2\theta = 25^\circ - 35^\circ$ range are L(115) at $2\theta = 27.56^\circ$ and H(0012) at $2\theta = 28.9^\circ$. The intensity of H(0012) increases with substitution ratio, but the intensity of the L(115) decreases with substitution up to $x = 0.15$.

The intensity of L(008) is decreasing with substitution, but for $x = 0.20$ ratio it has maximum value. In spite of this, the intensity of H(0010) is higher for samples B, C and D. The peak seen at $2\theta = 31.1^\circ$ was indicated as L(117). The intensity of this peak decreased with substitution ratio above $x = 0.05$ and showed a significant increase for $x = 0.20$ substitutional ratio. Another clear observation was found for the peak corresponding to $2\theta = 33.8^\circ$ labelled as H(0014). For unsubstituted sample this peak was not found while with increase in substitution, its intensity was increased. In accordance with the results obtained for the other peaks, this peak showed a decrease in intensity for $x = 0.20$ substitution ratio.

It can be seen from XRD patterns that with increase in substitution ratio of Zinc for Calcium, the intensities of the peaks corresponding to the high- T_c phase increase while those reflections corresponding to the low- T_c phase decrease. At the highest concentration of Zinc, the low- T_c phase reflections are predominant compared to the high- T_c phase reflections

In spite of multiphase nature of samples, it's possible to say that the dominant phase is high- T_c phase. The volume fraction of high- T_c phase (2223), which indicates the percentage of the reflections of 2223 phase in system, is calculated for all samples by using

$$f_{2223} = I_{H(0010)} / I_{H(0010)} + 0.8 I_{L(008)} \quad (3.1)$$

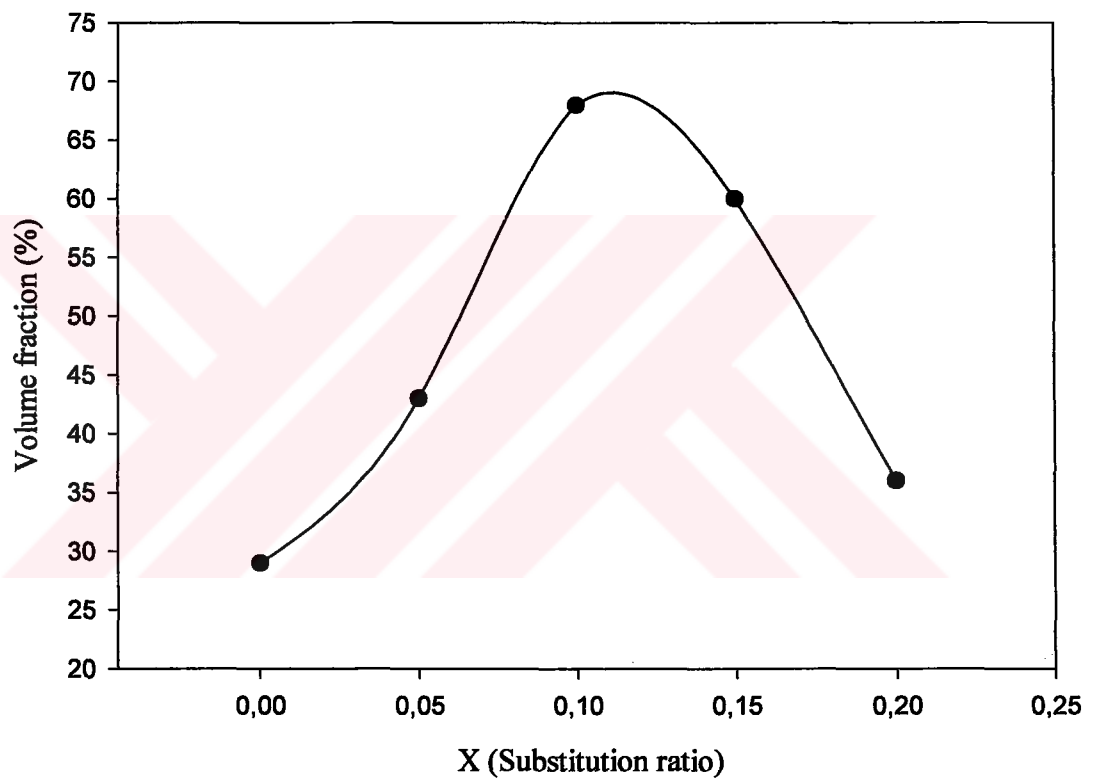


Figure 3.4. Volume fraction of ZnO substituted samples.

formula (Cooper et al., 2001). L(008) corresponds to $2\theta = 23.13^\circ$ and H(0010) to $2\theta = 23.97^\circ$. As shown in Figure 3.4, volume fraction is %68 for sample C and %60 for D which are in accordance with resistivity measurements. Volume fraction for A is %29, %43 for B and %36 for sample E.

Patterns obtained from XRD measurements provide knowledge not only for superconducting phases but also for not desired impurity phases. All ZnO samples show ZnO impurity at $2\theta = 36^\circ$, which increase with substitution ratio. Thus it could be said that ZnO does not enter in the crystal structure. Some of samples have CuO impurity at $2\theta = 38.8^\circ$.

It is well established that for an optimum hole concentration T_c has a maximum value and above and below this optimum, T_c decreases. The increase in the hole concentration might be responsible for improvement of the superconducting properties.

3. 2. 3. SEM Measurements

The microstructures of the top surfaces of all Zinc substituted samples are shown in SEM photographs taken at the same x2000 magnification in Figure 3.5. In all samples, the dominant structure is plate-like grains randomly distributed due to the presence of the pores in between the grains in these low-density compacts. A plate-like nature is typical of the superconducting phase (Kocabaş et al., 2000). Sample A and B have fine crystalline and homogeneous structure in needle-like and rood-like form. For samples C and D grains are in plate-like form, which is more preferable for superconductivity. This behaviour is attributed to increasing connectivity between the superconducting grains.

Sample E is also in plate-like form, but there is much more porosity between grains so the weak link nature of superconductivity can be observed which leads to depress in T_c . In conclusion C and D have better crystal structure than other samples,



Figure 3.5. a) Scanning electron microscope photographs of the top surfaces of ZnO substituted samples. Magnification X 2000.

[A(x=0.00), B(x=0.05), C(x=0.10)]

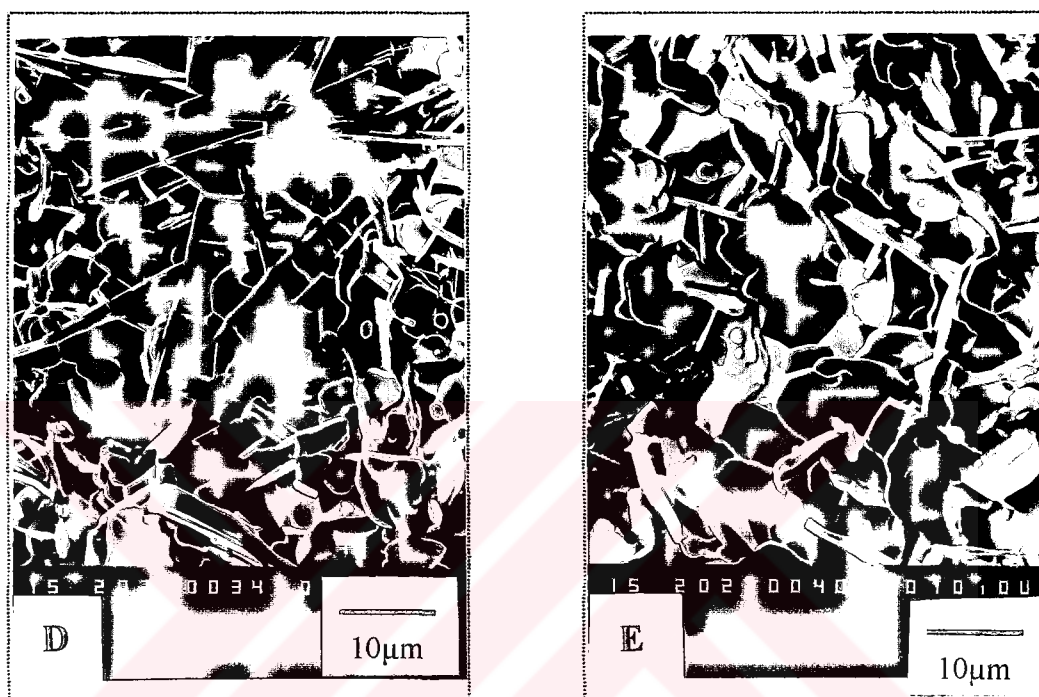


Figure 3.5. b) Scanning electron microscope photographs of the top surfaces of ZnO substituted samples. Magnification X 2000.

[D(x=0.15), E(x=0.20)]

that may be explanation for the greatest offset temperature (zero resistance temperature) behaviour.

The theoretical density of BPSCCO system is about 6,3 g/cm³ obtained from the lattice parameters (Yang X. & Chaki T.K., 1993). The density of pellets in this work were determined to be 5.02, 4.33, 4.79, 4.65 and 4.95 g/cm³ respectively from A to E, measured by water displacement Archimedes method using

$$\rho = \frac{W(a) \cdot \rho(fl)}{W(a) - W(fl)} \quad (3.2)$$

formula. $\rho(fl)$ is density of the liquid, $W(a)$ is weight of the solid in air and $W(fl)$ weight of the solid in liquid.

Most open pore volume was intruded by water during these tests (Kocabaş & Çiftçioğlu, 2000). The densities of the same pellets were estimated to be in the 3.4 to 4.0 g/cm³ range from their dimensional measurements. If the theoretical density of these pellets is taken as 6.3 g/cm³, this indicates that these pellets have %37 to %46 porosity. The bulk densities evaluated by water displacement technique are in the %68 to %79 range of theoretical density. This shows that about two fifth of the pores were filled by water during the density determinations.

3. 3. Effect of Silver(II)oxide Substitution

3. 3. 1. Resistivity Measurements

The temperature dependence of resistance of all samples is shown in Figure 3.6. in T= 80-220 K range. All samples display a metallic character above onset temperature. The onset temperature of samples is 117K, 121 K, 125 K, 123 K and 121 K respectively. Resistivity measurement results also showed that resistivity in the metallic character region for substituted samples are higher than the unsubstituted sample. The critical temperature, zero resistance temperature, of samples from A to E

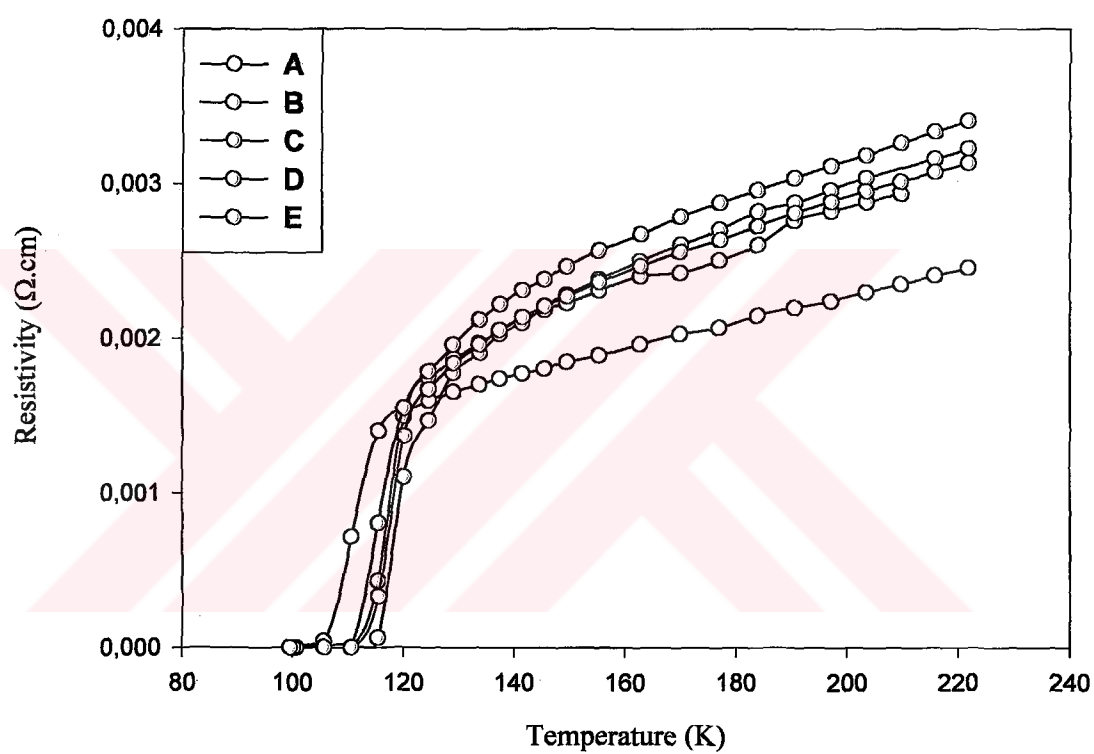


Figure 3.6. Resistivity curves of Ag_2O substituted samples.
A (x=0.00), B (x=0.05), C (x=0.10), D (x=0.15), E (x=0.20)

is 106 K, 110 K, 110 K, 115 K and 110 K respectively. Results obtained by Khan et al. (Khan & Khizar, 1999) for T_c at $x=0.05$ substitution for calcium are nearly the same to ours. The same composition was prepared by glass precursor method and samples were annealed at 850°C for 240h in air. They found that for undoped sample zero resistance temperature is 109 K while for $x=0.05$ substitution of Ag, T_c decreases to 106 K. In our study samples were annealed at 850°C for 250h in air and preparation method was different. Difference for T_c may be caused by these preparation conditions. Pb doped BSCCO (2223) system has 110 K offset temperature. Results obtained from four-probe point resistivity measurements are nearly to this value.

Rojek et al. (Rojek et al., 1989) reported that in $\text{Bi}_{1.4}\text{Pb}_{0.6}\text{Ag}_{0.2}\text{Sr}_2\text{Ca}_2\text{Cu}_3\text{O}_{10-x}$ composition, prepared by solid state reaction method, T_c values for 2, 4, 8 and 16 days annealing time, were measured as 108.5, 111.7, 112.8 and 114 K respectively. All samples show T_c onsets at about 119 ± 1 K. These results are in accordance with our results. Although we substituted calcium by zinc, the similar values for T_c and onset temperatures were obtained. This may be due to the slow reaction kinetics of formation for the high- T_c phase.

Matsushita et al. (Matsushita et al., 1994) studied the effect of Ag addition to $\text{Bi}_{2-x}\text{Pb}_x\text{Sr}_2\text{Ca}_2\text{Cu}_3\text{O}_y+\text{Ag}$ (0-100 wt %) system. For samples with 40-60 wt % Ag, where $x=0.7$, values of zero resistance higher than 110 K were obtained. It is likely that the role of Ag is to give better connectivity between the grains and drastically reduce resistivity.

Increasing in the substitution ratio of Ag_2O increases the offset temperature of samples. The highest value is for sample D ($x=0.15$) and so it could be said up to certain substitution ratio Ag_2O improves the formation of high- T_c phase. The transition width is 11 K, 11 K, 14 K, 8 K and 11 K respectively from samples A to E, which indicates that nearly pure structure is obtained.

3.3.2. X-ray Diffraction Measurements

The powder XRD patterns of all samples are given in Figure 3.7. The high- T_c and low- T_c phase peaks were identified by using the tables given by Bansal et.al. and Pandey et.al.(Appendix B). All samples have a multiphase nature with high and low- T_c peaks. Impurity phase CuO is showing at $2\theta = 38.8^\circ$ in all samples. There is also another impurity phase at $2\theta = 19.00^\circ$ which we couldn't able to named. The characteristic peaks of BSCCO system, L(002) and H(002), are not visible in all samples. The most visible peaks which can seen in $2\theta = 20^\circ$ - 35° are L(115) at in $2\theta = 27.6^\circ$ and H(0012) at in $2\theta = 28.09^\circ$. The intensity of L(115) decreases with substitution ratio, but intensity of H(0012) increases.

The peak corresponding to in $2\theta = 33.8^\circ$ is labelled as H(203). The intensity of this peak is increasing with substitution. In spite of this, intensity of the peak shown at in $2\theta = 31.1^\circ$ is decreasing with Ag_2O substitution. XRD patterns results revealed that number and intensities of the high- T_c reflections are predominant compared to the low- T_c phase reflections. These results show that Ag_2O substitution in BPSCCO ceramic stimulates a higher degree of orientation of grains of 2223 phase predominantly along the c-axis.

Khan et al. (Khan &Khizar, 1999) were reported that with the addition of Ag ($x=0.05$), only those peaks corresponding to the low- T_c phase were observed. It's well known that the volume fraction of the high- T_c phase increases with increase in sintering time, while the low- T_c phase decreases. Higher sintering time in our study could be reason for the large percentage of the high- T_c phase. It has been widely accepted that Ag addition in BPSCCO reduces the partial melting temperature of the system and thereby accelerates the formation rate of 2223 phase (Sobha at al., 1998).

In spite of multiphase nature of samples, the dominant phase is high- T_c phase. The volume fraction of 2223 phase was calculated by formula given before by using intensities of L(008) and H(0010) peaks. As shown in Figure 3.8.volume fraction is

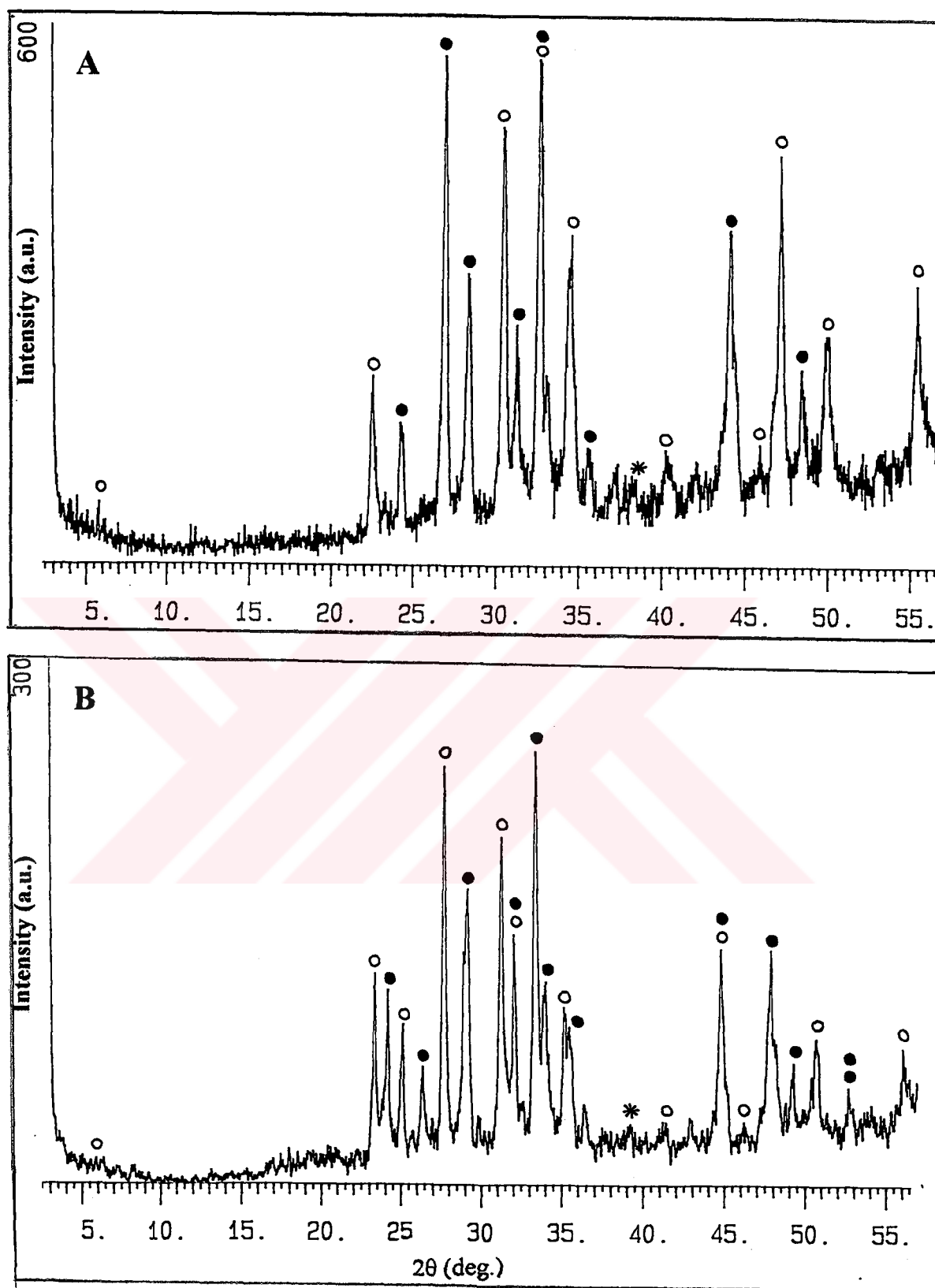


Figure 3.7.a) XRD patterns of Ag_2O substituted samples of $\text{Bi}_{1.7}\text{Pb}_{0.3}\text{Sr}_2\text{Ca}_{2-x}\text{Ag}_x\text{Cu}_3\text{O}_y$ system. [A ($x=0.00$), B ($x=0.05$)] \circ - Low- T_c phase; \bullet -High- T_c phase; $*$ - CuO; Δ - unknown phase

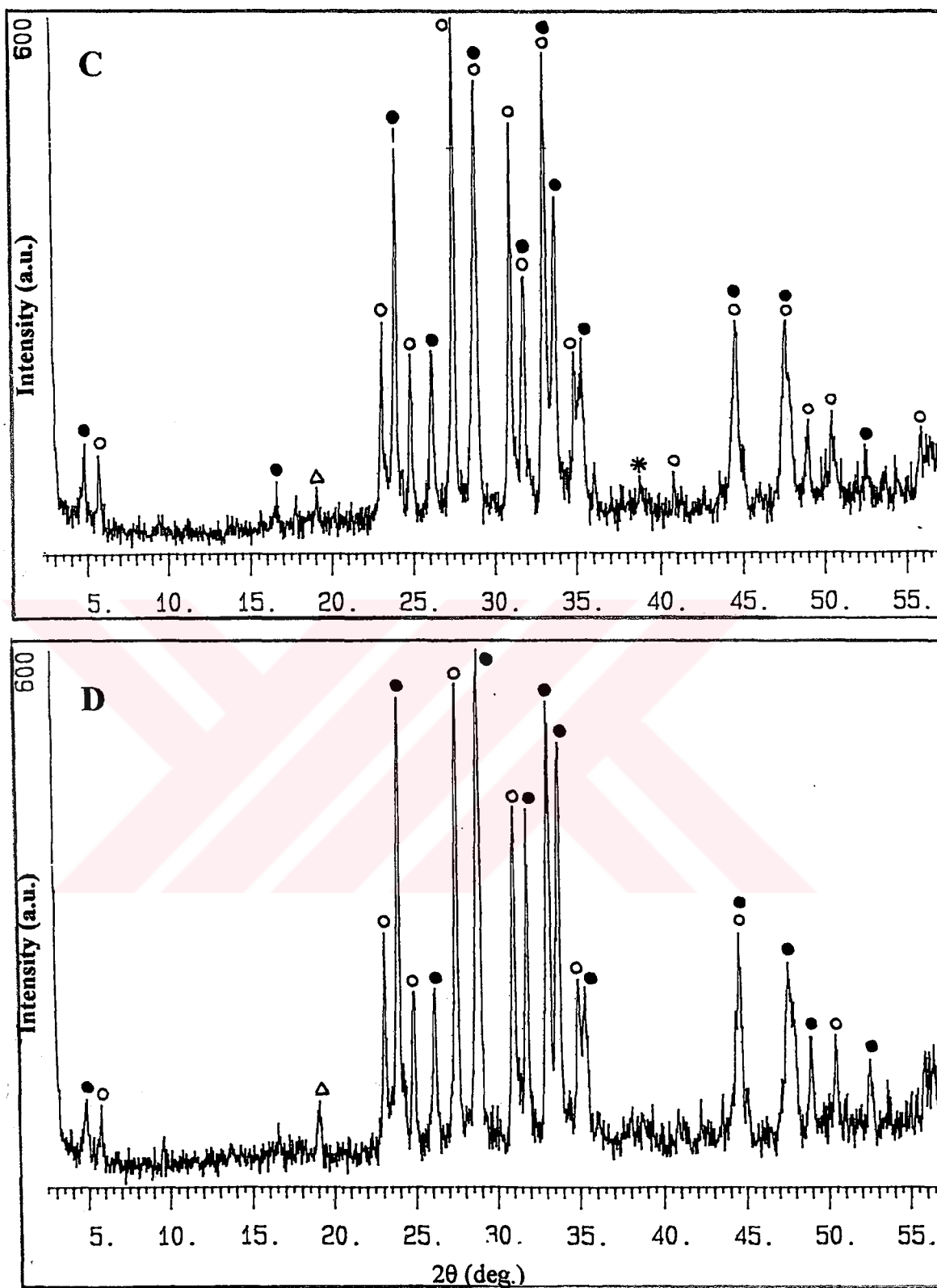


Figure 3.7.b) XRD patterns of Ag_2O substituted samples of $\text{Bi}_{1.7}\text{Pb}_{0.3}\text{Sr}_2\text{Ca}_{2-x}\text{Ag}_x\text{Cu}_3\text{O}_y$ system. [C ($x=0.10$), D ($x=0.15$)] ○- Low- T_c phase; ●-High- T_c phase; * - CuO; Δ - unknown phase

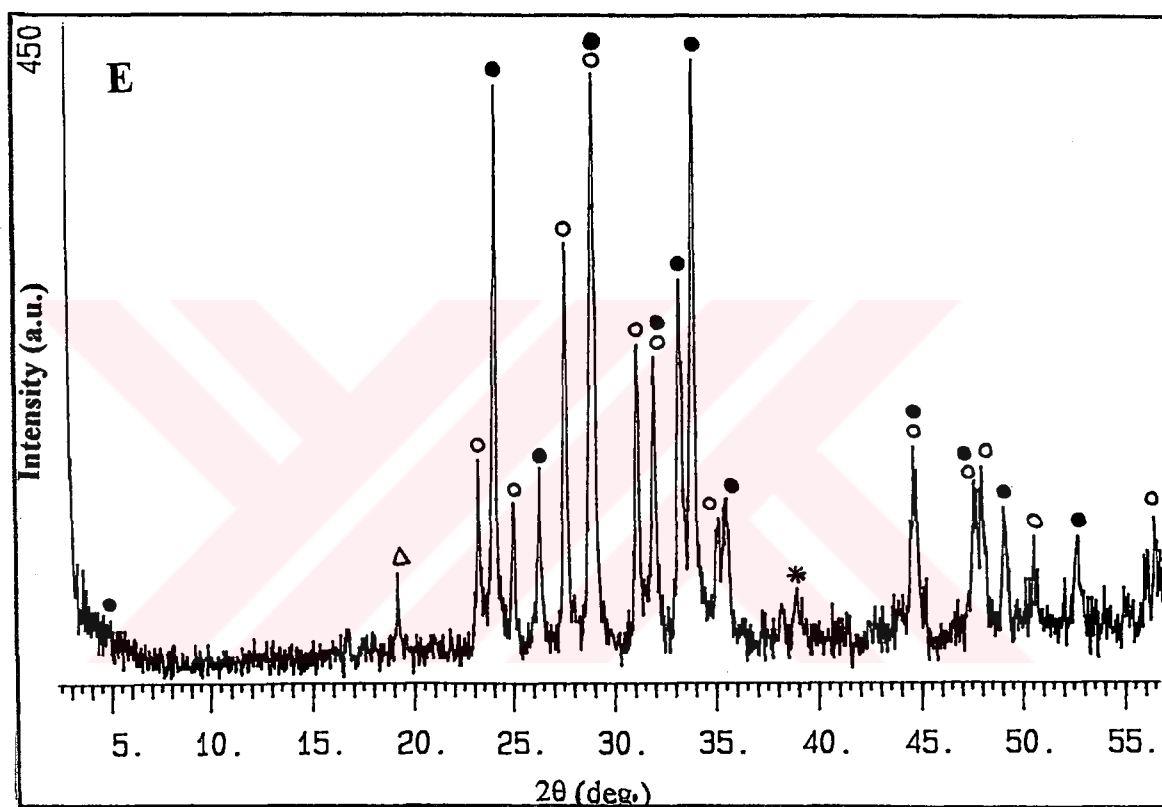


Figure 3.7.c) XRD patterns of Ag_2O substituted samples of $\text{Bi}_{1.7}\text{Pb}_{0.3}\text{Sr}_2\text{Ca}_{2-x}\text{Ag}_x\text{Cu}_3\text{O}_y$ system. [E ($x=0.20$)] ○- Low- T_c phase; ●-High- T_c phase; *- CuO ; Δ - unknown phase

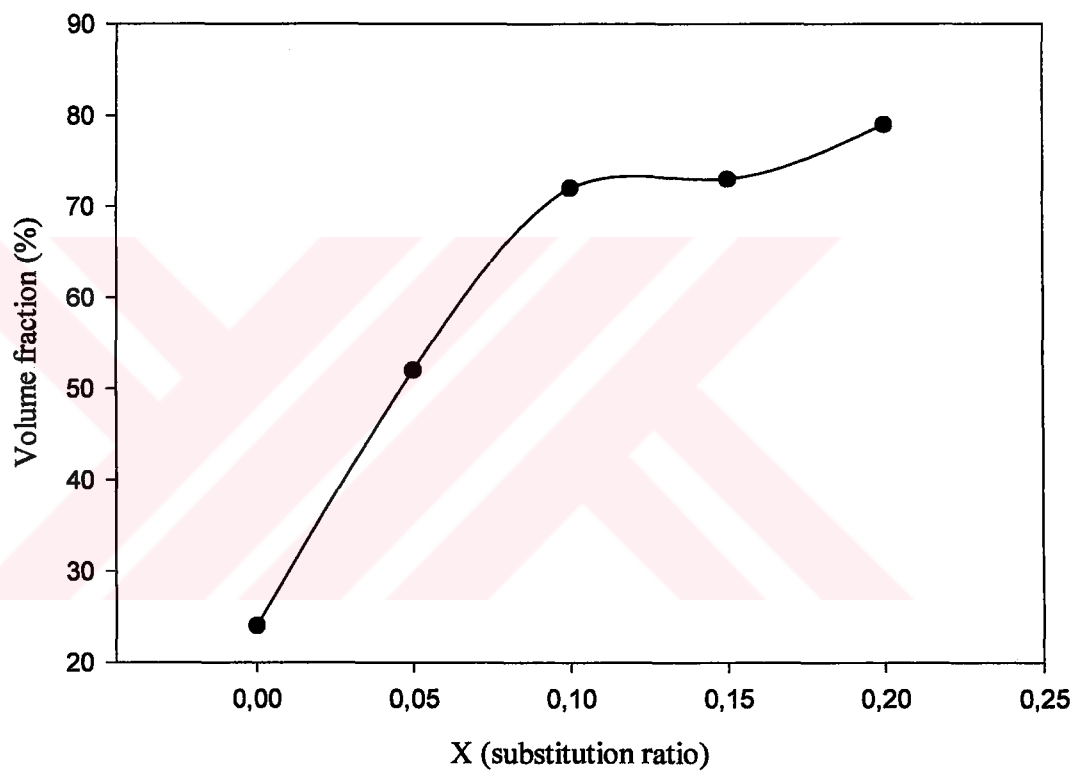


Figure 3.8. Volume fraction of Ag₂O substituted samples.

increasing with substitution ratio. Values obtained are %24, %52, %72, %73 and %79 respectively from sample A to E.

XRD measurements also provide knowledge about impurity phases. Impurity implicated the substituted Ag_2O wasn't seen in results lead to a conclusion that silver is not incorporated in the lattice.

3. 3. 3. SEM Measurements

The microstructures of the top surfaces of all samples are shown in Figure 3.9. SEM microphotographs are taken at x2000 magnification for all samples. Unsubstituted sample A has homogeneous structure in plate-like and needle-like form. With increasing substitution ratio, plate-like form could be seen much more evidently. The grain size is increasing also with substitution, which is in accordance with results obtained from resistivity measurements and XRD. Higher grain size provides stronger contact between grains, which leads to improvement in high- T_c phase. In sample E plate-like form of grains is dominant but there is also needle-like form.

The densities of samples were determined by Archimedes water displacement method. The density of pellets in this work were calculated to be 5.17g/cm^3 for $x=0.00$, 5.00 g/cm^3 for $x= 0.05$, 4.53 g/cm^3 for $x= 0.10$, 4.52 g/cm^3 for $x= 0.15$ and 4.89 g/cm^3 for sample E with $x=0.20$ substitution ratio. The densities of pellets were calculated to be in the 3.85 to 4.38 g/cm^3 range from dimensional measurements. If theoretical density is taken as 6.3 g/cm^3 , this indicates that pellets have %30 to %39 porosity.

Obtained results by water displacement technique are in the %72 to %82 range of theoretical density, which is calculated from the lattice parameters to be 6.3 g/cm^3 . This revealed that about one third of the pores were filled by water during water displacement density measurements.

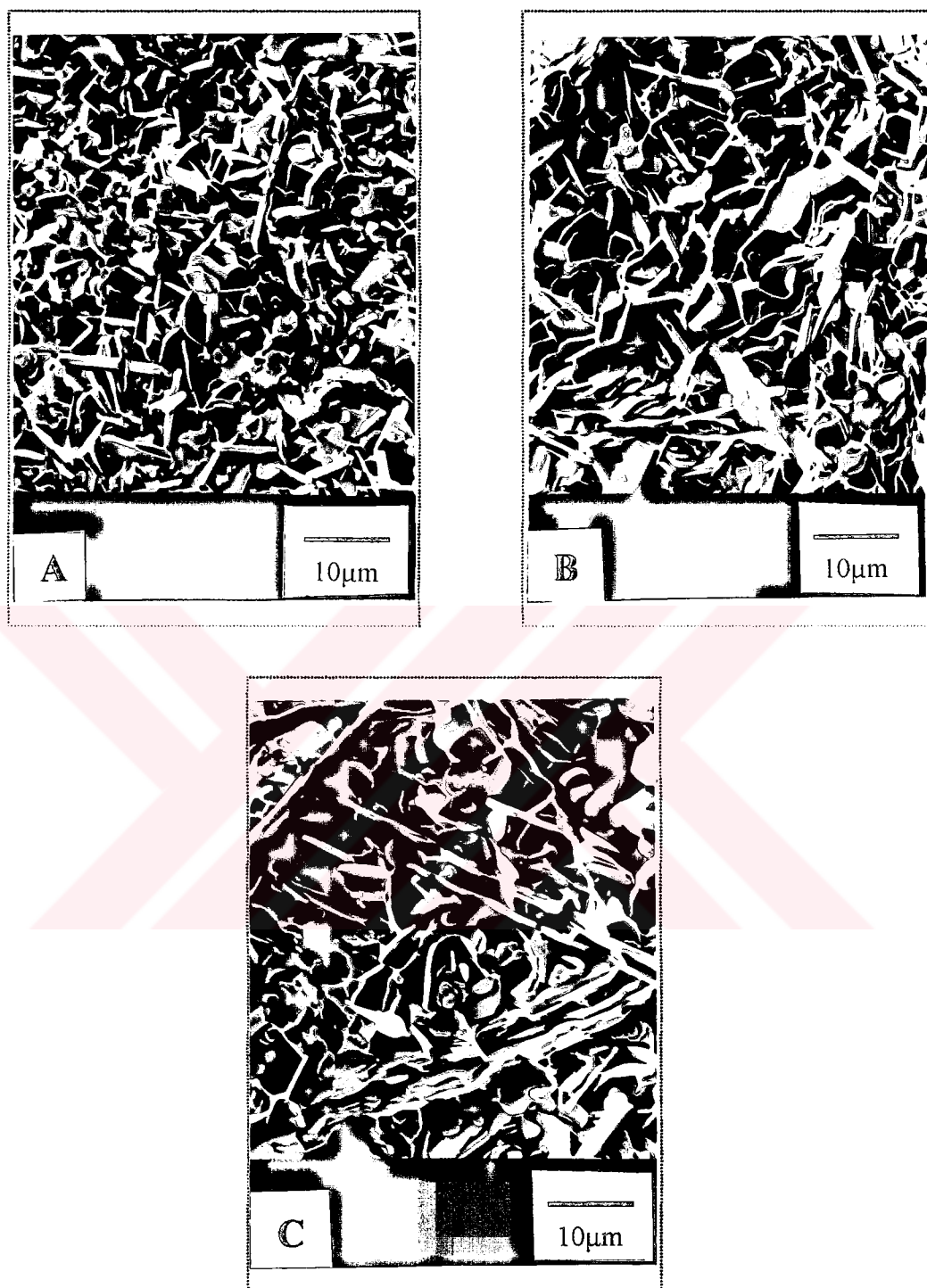


Figure 3.9. a) Scanning electron microscope photographs of the top surfaces of Ag_2O substituted samples. Magnification X 2000.

[A($x=0.00$), B($x=0.05$), C($x=0.10$)]

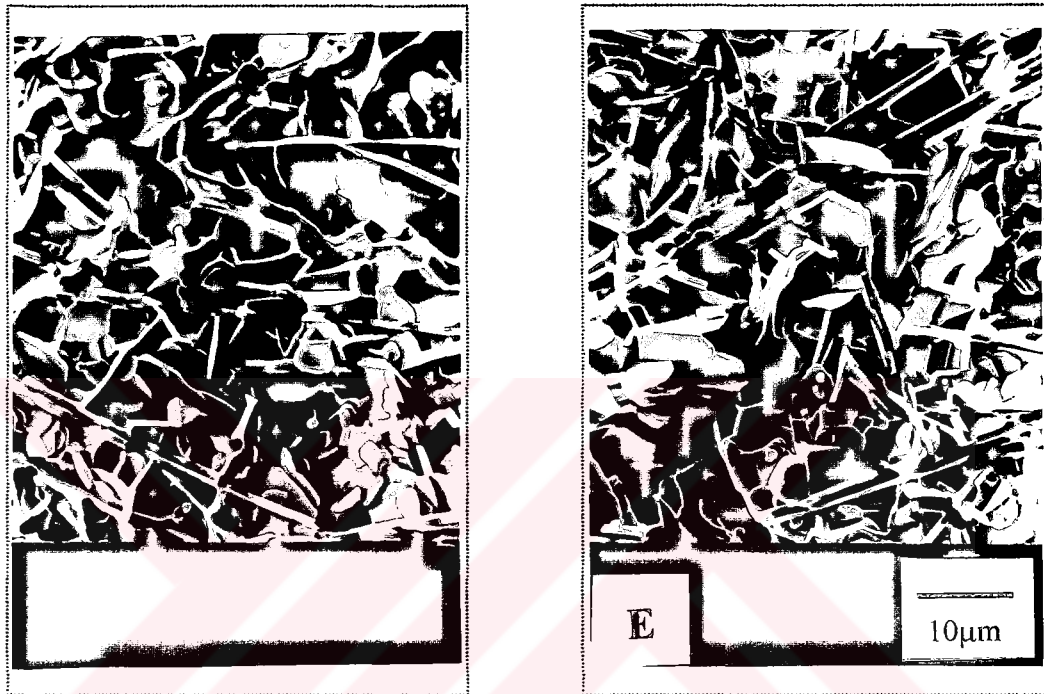


Figure 3.9. b) Scanning electron microscope photographs of the top surfaces of Ag₂O substituted samples. Magnification X 2000.

[D(x=0.15), E(x=0.20)]

3.4. Comparison of Results

In this research it was examined the effect of ZnO and Ag₂O partial substitution for Ca on the formation of the high-T_c phase in Bi_{1.7}Pb_{0.3}Sr₂Ca_{2-x}M_xCu₃O_y system. Zn²⁺ belongs to 2B transition elements group with 0.74Å ionic radii smaller than the ionic radii of Ca²⁺. Ca²⁺ is the element of alkaline-earth group which ionic radii is 0.99 Å. The other substituted element Ag¹⁺ is 1B group transition element with 1.26 Å ionic radii, higher than the Ca²⁺ radii. Substitution of elements with different ionic radii may be responsible for variation of the structure of system. Partial replacement of elements with smaller ionic radii is expected to be reason for decrease in the c-axis, which leads to decrease in T_c.

Obtained results show that both for ZnO and Ag₂O substitutions, zero resistance temperature and volume fraction values are maximum for the optimum substitution ratios. Zero resistance values for Ag₂O substitution are higher than the ZnO's so, it's possible to say that Ag₂O has better effects on the system properties. Volume fraction values, which indicate the percentage of high-T_c phase in the system, are also higher for Ag₂O substituted samples.

Comparison of the resistance behaviour of both substitutional groups, revealed that the resistivity values in the metallic character region for Ag₂O substituted samples are half of the values for ZnO group in the same region. This behaviour could be explanation of the higher T_c values for Ag₂O substituted samples.

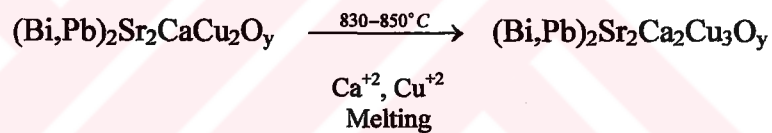
Transition width, a sign of pure structure of system, has lower values for Ag₂O substituted group. Because of all stated above we could say that Ag₂O play better role in improvement of the superconducting properties of the system than the ZnO.

Samples, prepared by the conventional solid state reaction method, were annealed at 850°C for 250h in air. XRD patterns of samples revealed various phases present in the crystalline samples. Although the multiphase nature of all samples in both

substitutional group, reflections corresponding to the high- T_c phase are predominant than the reflections of the low- T_c phase.

The density values, less than the theoretical density, are almost the same in both substitutional groups which indicates that the structure is in less compact form. Smaller density is sign of the pores in the between grains which effects T_c value negatively. The comparison of the superconducting parameters of system is given in Table 3.1.

When a particularly amount of Ag_2O and ZnO is added to (Bi,Pb)-2223 system, the liquid phase is established. This liquid results in the increment of T_c with the improvement of weak link of grain boundary. The formation of this liquid phase is believed to be an origin of the enhancement of the formation of the high- T_c phase. Consequently, the following reaction for the formation of high- T_c phase is proposed:



On the contrary to different ionic radii of substituted elements we could say that not only the difference of radii but also true valance of elements is responsible for variation of superconducting properties of system. The substitution of Ca^{2+} by the transition element Ag^{1+} causes decrease of electron density, which in turn increases the hole carrier concentration leading to an increase of the T_c and an improvement of the other superconducting properties. In contrary to the same valance of Zn^{2+} with Ca^{2+} , results in this part of research for T_c are almost the same with results given in literature, only for an optimum substitution ratio. If Zn is in the +2 state, then there will be no change in the carrier concentration, leads to a modification of the structure as the variation in T_c which can be due to the change in volume fraction of the 2223 phase as a result of substitution. So it's possible to say that the smaller ionic radii could be a reason for smaller zero resistance values than the Ag_2O .

Table 3.1. Comparison of characteristics obtained for ZnO and Ag₂O substituted samples.

Substitution Ratio	T _c (K)		T _{c onset} (K)		Volume Fraction (%)		Density (g/cm ³)	
	ZnO	Ag ₂ O	ZnO	Ag ₂ O	ZnO	Ag ₂ O	ZnO	Ag ₂ O
x=0.00	105	106	125	117	29	24	5.02	5.17
x=0.05	100	110	115	121	43	52	4.33	5.00
x=0.10	108	110	123	125	68	72	4.79	4.53
x=0.15	110	115	121	123	60	73	4.65	4.52
x=0.20	95	110	118	121	36	79	4.95	4.89

CHAPTER FOUR

CONCLUSIONS

4. 1. Conclusions

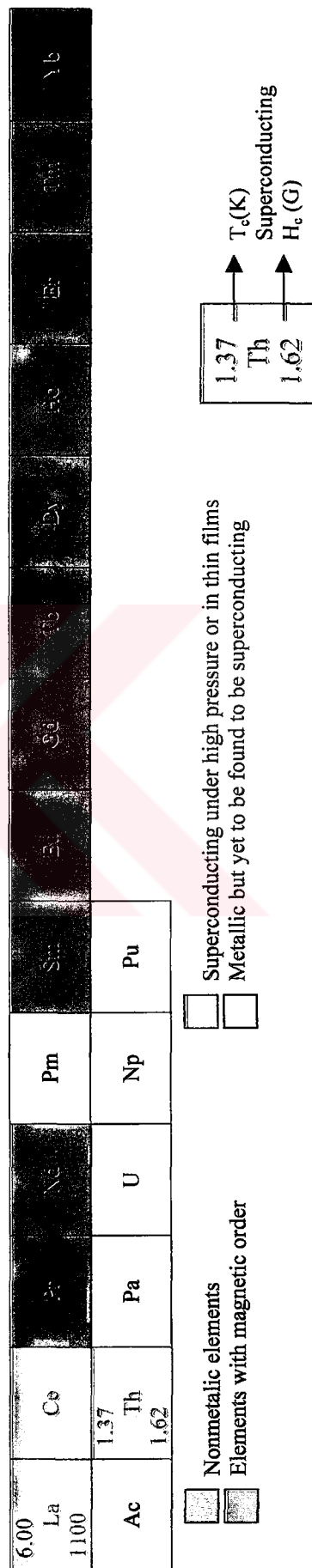
In order to stabilise the superconducting phase of the copper oxide based materials, elemental substitution method has been widely employed. The $(\text{Bi,Pb})_2\text{Sr}_2\text{Ca}_2\text{Cu}_3\text{O}_y$ type phase in pure form has 110 K superconducting transition temperature. However, this phase is not easily prepared in pure form. Partial substitutions by other elements at various metal sites in this system can stabilise the 2223 phase and improve its superconducting properties.

In this thesis, we have studied the effects on superconducting properties of elemental substitution of Ca by ZnO and Ag_2O , which has different ionic radii compare to Ca. Samples, prepared with substitutions at five different molar ratios have been characterised by resistivity-temperature measurement, X-ray diffraction patterns, scanning electron microscopy photographs and density measurement made by Archimedes water displacement method. Additional data about properties of the system were obtained by calculations of volume fraction of high- T_c phase. Comparison of the results for ZnO and Ag_2O substitutions, obtained from experimental measurements, were also made. Under this comparison the effects of each substitution on improvement and variation of system's properties were determined. In conclusion, the better substitution element was indicated, which is more favorable for a desirable improvement of system characteristics.

APPENDIX A

Periodic table of the elements showing superconducting metals with transition temperatures and critical fields. (Gladstone, Jensen & Schrieffer, 1969)

H																	He				
Li	Be															B	C	N	O	F	Ne
Na	Mg															1.14 Al 105	Si	P	S	Cl	Ar
K	Ca	Sc	0.39 Ti 100	5.38 V 1420	0.88 Zn 53				Cu	0.56 Cd 30				Ge	As	Se	Br	Kr			
Rb	Sr	Y	0.55 Zr 47	9.50 Nb 1980	0.92 Mo 95	7.77 Tc 1410	0.51 Ru 70	Rh	Pd	3.72 Sn 309				3.40 In 293	3.72 Sb 309	Te	I	Xe			
Cs	Ba	Lu	0.12 Hf 830	4.48 Ta 830	0.01 W 1.07	1.4 Re 198	0.66 Os 65	0.14 Ir 19	Pt	4.15 Hg 412				2.39 Tl 171	7.19 Pb 803	Po	At	Rn			
Fr	Ra																				



APPENDIX B

Calculated and observed d-spacings for powders after 48h sintering. Lines indexed with respect to 2212 unit cell with $a \cong b = 5.404 \text{ \AA}$, $c = 30.400 \text{ \AA}$ and 2223 unit cell with $a \cong b = 5.404 \text{ \AA}$, $c = 37.207 \text{ \AA}$ phases (CuK_α radiation)

hkl	d_{cal} (\AA)	d_{obs} (\AA)	2θ_{obs} (deg)	I/I_m (%)	hkl	d_{cal} (\AA)	d_{cal} (\AA)	2θ_{obs} (deg)	I/I_m (%)
H-002	18.514	18.395	4.800	7	H-1111	2.527	2.528	35.475	31
L-002	15.391	15.740	5.610	2	H-2010	2.184	2.184	41.305	5
L-008	3.800	3.823	23.250	6	H-2012	2.034	2.034	44.500	27
H-111	3.804	3.823	23.250	6	L-2020	2.0307	2.0309	44.580	32
H-0010	3.703	3.709	23.970	26	L-220	1.912	1.911	47.550	50
H-113	3.653	3.655	34.335	16	H-220	1.912	1.911	47.550	50
L-113	3.577	3.566	34.950	6	H-2014	1.891	1.892	48.040	24
H-115	3.398	3.395	26.225	52	H-1117	1.893	1.892	48.040	24
L-115	3.237	3.237	27.530	17	L-1115	1.791	1.805	50.515	3
H-117	3.099	3.098	28.795	80	H-1119	1.736	1.740	52.540	12
L-117	2.870	2.872	31.115	21	H-0022	1.683	1.698	53.955	5
H-119	2.801	2.801	31.925	58	H-315	1.666	1.665	55.105	9
L-200	2.704	2.702	33.125	100	H-317	1.627	1.627	56.525	20
H-200	2.704	2.702	33.125	100	H-319	1.579	1.579	58.395	10

REFERENCES

- Abd-Shukor, R. & Lo, S.V. (2001). Effect of Zn and Mn substitutions on the formation and superconductivity of Tl-1212 type phase $(\text{Tl}_{0.85}\text{Cr}_{0.15})\text{Sr}_2\text{CaCu}_2\text{O}_7$. J. Materials Science Letters, 20, 159-161
- Anis-Ur-Rehman, M. et al. (1998). Sintering effect on Bi(Pb)-Sr-Ca-Cu-O high- T_c superconductors. J. Materials Science, 33, 1789-1793
- Badica, P., Aldica, G. & Mandache, S. (2000). Sc addition to $(\text{Bi,Pb})_2\text{Sr}_2\text{Ca}_2\text{Cu}_3\text{O}_x$ freeze-dried ceramic. J. Superconductivity: Incorporating Novel Magnetism, 3, No:4, 529-533
- Bansal, S. et al., (1991). Pb-substituted $\text{Bi}_2\text{Sr}_2\text{Ca}_2\text{Cu}_3\text{O}_{10}$ ceramics. Physica C, 173, 260-266
- Bichhle, G.K. et al. (1991). Enhanced flux pinning by zinc substitution in $\text{YBa}_2\text{Cu}_3\text{O}_{7-\delta}$. Supercond. Sci. Techn., 4, 57-61
- Bourdillon, A. & Bourdillon, N. X. Tan. (1994). High Temperature Superconductors. USA: Academic Press.
- Chiu, Y.D. et al. (1994). Effect of Ag_2O on the formation of high- T_c phase in the $\text{BPSCCO}/\text{Ag}_2\text{O}$ composites. Physica C, 235-240, 485-486

- Cooper, H. et al. (2001). Phase transformation characteristics of BSCCO tapes processed via cryogenic and room temperature pressing. Supercond. Sci. Techn., 14, 533-538
- Cömert, H. et al. (1994). The effect of Ag diffusion on the crystal structure and electrical properties of Bi(Pb)SrCaCuO superconductors. Supercond. Sci. Techn., 7, 824-827
- Demirel, A.I. (1995). Preparation and Characterization of YBCO Thin Film by Using Specific MOCVD Growth Technique. Bristol: Ph.D. Thesis.
- Gladstone, G., Jensen, M.A. & Schrieffer, J.R. ; Parks, R.D. (Eds.). (1969). Superconductivity (vol. 2). New York: Marcel Dekker, Inc.
- Guo, Y.C., Liu, H.K. & Dou, S. X. (1994). Effect of silver additions on properties of (Bi,Pb)₂Sr₂Ca₂Cu₃O₁₀/Ag high-temperature superconducting tapes. Materials Letters, 18, 336-340
- Gupta, R.P. & Gupta, M. (1998). Effect of zinc substitution on the carrier density in YBa₂Cu₃O_{7-δ} superconductors. Physica C, 305, 179-184
- Halim, S.A. et al. (1999). Effect of Ba and Zn doping in Bi₂Pb_{0.6}Sr₂Ca₂Cu₃O₈ superconductors using ac susceptibility measurements. J. Materials Science, 34, 2813-2819
- Hu, W.-Z. et al. (2000). Synthesis and superconductivity of Zn-substituted HgBa₂CuO_{4+δ} with various doping levels. Physica C, 338, 72-75
- Jenkins, R. & Snyder, R.L. (1996). Introduction to X-ray Powder Diffractometry. USA: John Wiley & Sons, Inc.

Kazakov, S. M. et al. (2001). Substitution effect of Zn and Cu in MgB_2 on T_c and structure. Solid State Communications, 119, 1-5.

Khan, M. N. & Kayani, A. N. (1998). Fabrication and transport properties of long-length doped $\text{Bi}_{1.7}\text{Pb}_{0.3}\text{Sr}_2\text{Ca}_{2-x}\text{M}_x\text{Cu}_3\text{O}_y$. J. Materials Science, 33, 2365-2369

Khan, M.N., Kayani, A.N. & ul Haq, A. (1997). Electronic structure and superconducting properties of doped BPSCC (2223) system. Physica C, 282-287, 869-870

Khan, M.N. & Khizar, M. (1999). Effect of rare-earth (Eu, Yb and Ag) substitutions on superconducting properties of the $\text{Bi}_{1.7}\text{Pb}_{0.3}\text{Sr}_2\text{Ca}_{2-x}\text{R}_x$ (R=Eu, Yb and Ag) Cu_3O_x system. J. Materials Science, 34, 5833-5838

Kocabaş, K & Çiftçioğlu, M. (2000). The effect of Sb substitution of Cu in $\text{Bi}_{1.7}\text{Pb}_{0.3}\text{Sr}_2\text{Ca}_2\text{Cu}_{3-x}\text{Sb}_x\text{O}_y$ superconductors. Phys. Stat. Sol. (a), 177, 539-545

Kocabaş, K. et al. (2000). The effect of Ag substitution of Cu in BPSCCO superconductors. Balkan Physics Letters, 8(1), 26-32

Kocabaş, K. & Kazancı, N. (1996). Superconductivity in Ag added Bi-Pb-Sr-Ca-Cu-O system. Tr.J.Physics, 20, 500-507

Kocabaş, K. (1994). Preparation of Pb-doped BiSrCaCuO superconducting ceramics. Tr. J. Physics, 18, 415-422

Kresin, V. Z. & Wolf, S. A. (1990). Fundamentals of Superconductivity. New York: Plenum Press.

Li, A. et al. (1999). Effect of zinc substitution on internal friction in YBCO superconductors. Supercond. Sci. Techn., 12, 645-648

- Maeda, H. & Togano, K. (1996). Bismuth-Based High-Temperature Superconductors. USA: Marcel Dekker, Inc.
- Matsushita, T. et al. (1994). The effect of Ag on the superconductivity of $\text{Bi}_{2-x}\text{Pb}_x\text{Ca}_2\text{Cu}_3\text{O}_y$ superconductors prepared by an optimum thermal procedure. Supercond. Sci. Techn., 7, 222-226
- Muralidhar, M. et al. (1994). A.c. and d.c. susceptibility studies on silver-doped BPSCCO (2223) superconductors. Materials Science and Engineering, B26, 151-155
- Muralidhar, M. et al. (1994). Elastic and plastic behaviour of lead and silver doped Bi-Sr-Ca-Cu-O superconductors. Materials Science and Engineering, B13, 215-219
- Nezir, S. (1996). Amonyum Nitrat Yöntemiyle Hazırlanmış Yüksek Sıcaklık Bi(Pb)-Sr-Ca-Cu-O Süperiletken Bileşiklerin Bazı Elektriksel, Yapısal ve Magnetik Özellikleri. Trabzon: Doktora Tezi.
- Padam, G. K. et al. (1991). Transformation of 2212 to 2223 phase in the Bi-Sr-Ca-O system. Solid State Communication, 80, No:4, 271-275
- Pandey, D. et al. (1991). Synthesis of $\text{Bi}_{1.6}\text{Pb}_{0.4}\text{Sr}_2\text{Ca}_2\text{Cu}_3\text{O}_y$ composition. Physica C, 173, 476-486
- Park, T. K. et al. (1999). Suppression of antiferromagnetic spin fluctuation in Zn-substituted $\text{YBa}_2\text{Cu}_3\text{O}_7$. Physica C, 320, 245-252
- Poole, C.P., Farach, H. & Creswick, R. J. (1995). Superconductivity. USA: Academic Press.

- Ravinder Reddy, R. et al. (1995). The relationship between the porosity and elastic moduli of the Bi-Pb-2212 high- T_c superconductor. Supercond. Sci. Techn., **8**, 101-107
- Rojek, A. et al. (1989). 115 K superconductivity in B-Pb-(Ag, Nb, Sb)-Sr-Ca-Cu-O systems. Solid State Communications, **72** (1), 113-116
- Romanenko, A. I. et al. (2000). Effect of oxygen redistribution in Bi-based high- T_c superconductors on their normal and superconducting properties. Physica C, **337**, 327-330
- Rose-Innes, A. C. & Rhoderick, E. H. (1980). Introduction to Superconductivity. (2th ed.). Great Britain: Pergamon Press Ltd.
- Schmidt, V. V., Müller, P. & Ustinov, A. V. (Eds). (1997). The Physics of superconductors. Germany: Springer – Verlag.
- Sobha, A. et al. (1998). Phase evolution in Ag, Ag₂O and AgNO₃ added (Bi,Pb)-2223 superconductor. Physica C, **307**, 277-283
- Suzuki, Y., Inoue, T. & Hayashi, S. (1989). Synthesis and decomposition of the high- T_c phase of a Pb-doped Bi-Sr-Ca-Cu-O superconductors. Japanese J. Applied Physics, **28** (8), L 1382-L 1384
- Tepe, M. & Abukay, D. (1997). Influence of Zn doping on the magnetic and electrical properties of Bi(Pb)SrCaCuO superconductors. Tr.J. Physics, **21**, 1010-1016
- Uluğ, A. (1994). Y₃Ba₄Cu₇O_x Bileşiğinin Sentezlenerek Yapısal ve Elektriksel Özelliklerinin İncelenmesi. Malatya: Doktora Tezi.

- Waldram, J. R. (1996). Superconductivity of Metals and Cuprates. Bristol: IOP Publishing Ltd.
- Yang, X. & Chaki, T.K. (1993). Hot rolling of $\text{Bi}_{1.6}\text{Pb}_{0.4}\text{Sr}_2\text{Ca}_2\text{Cu}_3\text{O}_x$ superconducting pellets. Supercond.Sci.Techn., 6, 343-348
- Yavuz, M. et al. (1998). Phase development and kinetics of high temperature Bi-2223 phase. J. Alloys and Compounds, 281, 280-289
- Yu, Y. et al. (1997). T_c enhancement in silver substituted $\text{Bi}_{1.7}\text{Pb}_{0.3}\text{Sr}_{2-x}\text{Ag}_x\text{Ca}_2\text{Cu}_3\text{O}_y$ Physica C, 282-287, 845-846

